

Quantum search with hybrid adiabatic–quantum walk algorithms and realistic noise

James G. Morley,^{1,*} Nicholas Chancellor,² Sougato Bose,¹ and Viv Kendon^{2,†}

¹*Department of Physics, UCL, Gower Street, London, UK*

²*Department of Physics, Durham University, South Road, Durham, UK*

(Dated: September 1st, 2017)

Computing using a continuous-time evolution, based on the natural interaction Hamiltonian of the quantum computer hardware, is a promising route to building useful quantum computers in the near-term. Adiabatic quantum computing, quantum annealing, computation by continuous-time quantum walk, and special purpose quantum simulators all use this strategy. In this work, we carry out a detailed examination of adiabatic and quantum walk implementation of the quantum search algorithm, using the more physically realistic hypercube connectivity, rather than the complete graph, for our base Hamiltonian. We interpolate between adiabatic and quantum walk searching, obtaining a family of hybrid algorithms. We show that all of these hybrid algorithms provide the quadratic quantum speed up with optimal parameter settings, which we determine and discuss in detail. We incorporate the effects of multiple runs of the same algorithm, noise applied to the qubits, and two types of problem misspecification, determining the optimal hybrid algorithm for each case. Our results reveal a rich structure of how these different computational mechanisms operate and should be balanced in different scenarios. For large systems with low noise and good control, quantum walk is the best choice, while hybrid strategies can mitigate the effects of many shortcomings in hardware and problem misspecification.

CONTENTS

I. Introduction	1
II. Background	2
A. Encoding search into quantum states	2
B. Quantum walk search algorithm	2
C. Adiabatic quantum search algorithm	4
D. Optimising annealing schedules	5
III. Generalized annealing schedules	6
A. Motivation and derivation	6
B. Numerical methods	7
C. Small system examples	8
IV. Performance of hybrid algorithms	9
A. Minimum gap scaling	9
B. Single avoided crossing model	11
C. Optimizing hybrid schedules for a single run	13
V. Multiple runs for one search	15
A. Motivation	15
B. Multiple run searching	15
C. Noisy quantum searching	16
VI. Problem misspecification	18
A. Motivation	18
B. Error in gap size	18
C. Error in avoided crossing location	18
VII. Conclusion	19

Acknowledgments

20

References

20

I. INTRODUCTION

Quantum computing based not on discrete quantum gates, but on continuous-time evolution under quantum Hamiltonians applied to qubits, is a promising route towards near-future useful quantum computers. This is in part because of the success of experimental quantum annealing efforts [1–5], and also because of special purpose quantum simulators that employ this technique, and are potentially useful for a wider range of computations [6]. Problems suitable for continuous-time algorithms are wide-ranging across many important areas, including finance [7], aerospace [8], machine learning [9–11], pure computer science [12], decoding of communications [13] and even computational biology [14].

Continuous-time computation is less familiar than the digital computation that is ubiquitous today, underpinning everything from mobile phones to internet servers. There is no classical equivalent to computing via continuous-time control of digital data to guide our intuition, or provide a source of classical algorithmic resources that might be adapted to a quantum setting. A detailed study based on a well-characterised problem can thus serve to elucidate the mechanisms in continuous-time quantum computing and build a firm foundation for further development. Hence, we have focused this work on the unordered search problem first studied in a quantum setting by Grover in 1997 [15]. Grover’s algorithm provides a quadratic speed up over classical searching, proved by Bennett et al. [16] to be the best possible improvement.

* james.morley.15@ucl.ac.uk

† viv.kendon@durham.ac.uk

Two further examples of quantum search algorithms are *quantum walk* (QW) searching [17] and the *adiabatic quantum computing* (AQC) search algorithm [18], which both obtain the optimal quadratic speed up. There remains the question of which is more efficient in terms of the prefactors [19], or more robust in the face of imperfections. While the results in [16] imply that any protocol we develop here will not provide better scaling properties, asymptotic scaling factors don't give a full account of algorithm performance. A recent study in which a quantum annealer appears to show the same asymptotic scaling as a classical algorithm, but with a prefactor advantage of $\sim 10^8$ [3], underscores the importance of practical computational advantages beyond asymptotic scaling. This prompts more detailed study of exactly how the algorithms work, the topic of many papers since the original algorithms were first presented.

Quantum walk searching has been shown to implement a similar type of rotation in Hilbert space that Grover's algorithms employs [17]. On the other hand, adiabatic quantum searching alters the Hamiltonian over time, turning on the term for the marked state slowly enough to keep the quantum system in its ground state throughout. On the face of it, these are quite different dynamics, as has been highlighted in [20]. However, both use the same Hamiltonians and initial states, and we argue here that both are best viewed as extreme cases of possible quantum annealing schedules. This invites consideration of intermediate quantum annealing schedules, and we show how to interpolate smoothly between them, enabling both mechanisms to contribute to solving the search problem. We examine the hybrid algorithms thus created using simplified models for the asymptotic scaling, and numerical simulation to explore smaller systems where more complex finite size effects contribute. Taking into account realistic factors, such as a finite initialisation time for each run of the algorithm, our results reveal a rich structure of intermediate strategies available to optimise the performance of a practical quantum computer.

Our paper is structured as follows. In Sec. II, we give the background and lay the groundwork for our study in terms of the QW and AQC protocols which we interpolate between. In Sec. III, we construct interpolated protocols which can take advantage of both QW and AQC mechanisms. We introduce three AQC schedules and corresponding hopping rates γ for QW which we use in this study, and we explain in detail how they arise from the dynamics of the quantum search Hamiltonian on a hypercube. We then turn to the performance of the interpolated protocols in finite-sized systems. In Sec. IV, we examine the scaling for larger systems in detail, and demonstrate that the interpolated protocols will also yield a quadratic speed up over classical searching. In Sec. V we incorporate strategies which involve performing multiple runs, including in Sec. VC the effect of adding decoherence, and in Sec. VI we examine the effect of problem misspecification. Finally in Sec. VII we summarise our results and their implications for future

work.

II. BACKGROUND

A. Encoding search into quantum states

The search problem can be framed in terms of the $N = 2^n$ basis states of an n -qubit system $\{|j\rangle\} = \{|0\rangle, |1\rangle\}^{\otimes n}$, where $\{|0\rangle, |1\rangle\}$ is the basis of a single qubit. We are given that one of the basis states behaves differently to the others and denote this 'marked' state as $|m\rangle$, where m is an n -digit bitstring identifying one of the basis states. Because of the difference in behaviour we can easily verify whether a given state is the marked state. The search problem is then to determine which of the basis labels j corresponds to the marked state label m , given that *a priori* we have no knowledge of m . We represent this ignorance of the marked state by beginning with the system in a uniform superposition over the basis states,

$$|\psi_{\text{init}}\rangle = \frac{1}{\sqrt{N}} \sum_{j=0}^{N-1} |j\rangle. \quad (1)$$

The quantum search algorithms considered in this paper solve the search problem by evolving the system into a state with a large overlap with the marked state, so that a measurement can be made to return the marked state label m with high probability. This is achieved by applying a (sometimes time-dependent) Hamiltonian to evolve the system initially in state $|\psi_{\text{init}}\rangle$ to a final state $|\psi_{\text{final}}\rangle$. Performing a measurement of this state in the basis $\{|j\rangle\}$ will yield the marked state label with probability $|\langle\psi_{\text{final}}|m\rangle|^2$. If $|\langle\psi_{\text{final}}|m\rangle|^2 = 1$ then the search is perfect and the problem is solved. If the search is imperfect then the problem can be solved by searching multiple times: since the result of each search is checked independently, a single successful search is sufficient. As long as $|\langle\psi_{\text{final}}|m\rangle|^2$ is greater than $1/\text{POLY}(n)$ this form of amplitude amplification will be efficient.

B. Quantum walk search algorithm

A continuous-time quantum walk can be defined by considering the labels j of the n -qubit basis states $\{|j\rangle\}$ to be the labels of vertices of an undirected graph G . The edges of G can be defined through its adjacency matrix A , whose elements satisfy $A_{jk} = 1$ if an edge in G connects vertices j and k and $A_{jk} = 0$ otherwise. Since G is undirected, A is symmetric, hence it can be used to define a Hamiltonian. Although we can use the adjacency matrix A directly, it is in general more convenient mathematically to define the Hamiltonian of the quantum walk using the Laplacian $L = A - D$, where D is a diagonal matrix with entries $D_{jj} = d_j$ the degree of vertex j in the graph. We follow this convention here, but note that in this work we use regular graphs for which the degree

$d_j = d$ is the same for all vertices, so that $D = d\mathbb{1}$, where $\mathbb{1}$ is the identity matrix (ones on the diagonal) of the same dimension as A . Terms proportional to the identity in the Hamiltonian shift the zero point of the energy scale and contribute an unobservable global phase, but otherwise don't affect the dynamics. The quantum walk Hamiltonian is then defined as $\hat{H}_{\text{QW}} = -\gamma\hat{L}$, where \hat{L} is the Laplacian operator, and the prefactor γ is the hopping rate of the quantum walk. We thus have

$$\hat{H}_{\text{QW}} = \gamma \left(d\hat{\mathbb{1}} - \sum_{jk} A_{jk}|j\rangle\langle k| \right) \equiv \gamma(d\hat{\mathbb{1}} - \hat{A}), \quad (2)$$

where the adjacency operator \hat{A} has matrix elements in the vertex basis $\{|j\rangle\}$ given by the adjacency matrix A . The action of \hat{H}_{QW} is to move amplitude between connected vertices, as specified by the non-zero entries in A . During a quantum walk, a pure state $|\psi(0)\rangle$ evolves according to the Schrödinger equation to give

$$|\psi(t)\rangle = \exp\{-i\hat{H}_{\text{QW}}t\}|\psi(0)\rangle \quad (3)$$

after a time t , where we have used units in which $\hbar = 1$.

Quantum walk dynamics can be used to solve the search problem by modifying the energy of the marked state $|m\rangle$ to give a quantum walk search Hamiltonian

$$\hat{H}_{\text{QWS}} = \gamma(d\hat{\mathbb{1}} - \hat{A}) - |m\rangle\langle m|. \quad (4)$$

Applying \hat{H}_{QWS} to the search initial state $|\psi_{\text{init}}\rangle$, Eq. (1), produces a periodic evolution such that the overlap with the marked state oscillates. The frequency of these oscillations depends on the hopping rate γ , which must be chosen correctly, along with the measurement time t_f , to maximize the final success probability $|\langle\psi(t_f)|m\rangle|^2$, where $|\psi(t_f)\rangle = \exp\{-i\hat{H}_{\text{QWS}}t_f\}|\psi_{\text{init}}\rangle$ is the state at time t_f .

The performance of quantum walk search algorithms will clearly have some dependence on the choice of the graph G . Provided the connectivity isn't too sparse or low-dimensional [21], most choices of graph will work, even random graphs [22]. Two convenient choices on which the quantum walk is analytically solvable are the complete graph, for which all vertices are directly connected, and a graph whose edges form an n -dimensional hypercube (see Moore and Russell [23] for details of quantum walks on hypercubes). We choose a hypercube, rather than a fully-connected graph, because it is the more practical graph in terms of implementation on a quantum computer. A hypercube graph corresponds to a transverse-field driver Hamiltonian which can be experimentally realized on a large scale [24]. The scaling arguments we give in this work also hold in the case of a fully connected graph, and could also be easily extended to a more general setting, for example to the 'typical' random graphs considered in [22].

The adjacency matrix of an n -dimensional hypercube graph has elements $A_{jk} = 1$ if and only if the vertex labels

j and k have a Hamming distance of one. That is, when written as n -digit bitstrings, they differ in exactly one bit position. The corresponding adjacency operator can be conveniently expressed as $\hat{A} = \sum_{j=1}^n \hat{\sigma}_x^{(j)}$, where the sum is over all n qubits and $\hat{\sigma}_x^{(j)}$ is the Pauli- X operator¹ applied to the j th qubit with the identity operator on the other qubits. That is,

$$\hat{\sigma}_x^{(j)} = \left(\bigotimes_{r=1}^{j-1} \hat{\mathbb{1}}_2 \right) \otimes \hat{\sigma}_x \otimes \left(\bigotimes_{r=j+1}^n \hat{\mathbb{1}}_2 \right), \quad (5)$$

where \otimes denotes the tensor product, and $\hat{\mathbb{1}}_2$ is the identity operator of dimension two. The Hamiltonian for the quantum walk search on the hypercube is then given by

$$\hat{H}_{\text{QWS}}^{(h)} = \gamma \left(n\hat{\mathbb{1}} - \sum_{j=1}^n \hat{\sigma}_x^{(j)} \right) - |m\rangle\langle m| \quad (6)$$

since an n -dimensional hypercube has vertices of degree n .

Childs and Goldstone [21] analyze the quantum walk search algorithm for both the complete and hypercube graphs. For each graph, they find optimal values of γ for which the performance of the search matches the quantum speed up achieved by the Grover search algorithm. Note that the initial state $|\psi_{\text{init}}\rangle$ from Eq. (1) is the (non-degenerate) ground state of both the hypercube and the complete graph Hamiltonians, i.e., $\hat{H}_{\text{QW}}^{(h)}$, without the marked state term. The marked state $|m\rangle$ is, by design, the ground state of the marked state component of the search Hamiltonian. For large values of γ , the marked state term is relatively small so the graph Hamiltonian dominates, and the ground state of the full search Hamiltonian $\hat{H}_{\text{QWS}}^{(h)}$ is approximately $|\psi_{\text{init}}\rangle$. Conversely, for small values of γ , the ground state of $\hat{H}_{\text{QWS}}^{(h)}$ is approximately $|m\rangle$. For intermediate values of γ , the ground state switches between the two over a narrow range. By calculating the energy spectrum of $\hat{H}_{\text{QWS}}^{(h)}$, Childs and Goldstone tune γ until both the initial state $|\psi_{\text{init}}\rangle$ and the marked state $|m\rangle$ have significant overlap with both the ground state E_0 and the first excited state E_1 of the search Hamiltonian. Intuitively, we want the search Hamiltonian to drive transitions between $|\psi_{\text{init}}\rangle$ and $|m\rangle$ as efficiently as possible. This occurs when the overlaps are evenly balanced, which in turn occurs when the gap $g = E_1 - E_0$ between the ground and first excited state is smallest. The time it takes for the transition to occur is proportional to $1/g$. For the hypercube graph, the

¹ Note that our definition of $\hat{\sigma}_x = \begin{pmatrix} 0 & 1 \\ 1 & 0 \end{pmatrix}$ differs from that used in [21, 25] by a factor of 2.

optimal value of γ is

$$\gamma_h^{(o)} = \frac{1}{2^{(n+1)}} \sum_{r=1}^n \binom{n}{r} \frac{1}{r}, \quad (7)$$

which differs from Eq. (12) in Ref. [21] due to our different definition¹ of $\hat{\sigma}_x$. The time to reach the first maximum overlap with the marked state is $t_h^{(o)} \simeq (\pi/2)\sqrt{N}$, providing a quadratic speed up equivalent to Grover's original search algorithm.

In general, problems with full permutation symmetry, such as the search problem, are considered to be toy problems from a practical point of view. A naive implementation of such a problem requires exponentially many terms of the form $\prod_{j \in q} \hat{\sigma}_z^{(j)}$, where q is a binary number with n bits, and j iterates over the bits in q that are equal to one. However, it has recently been shown that the spectrum of such terms in permutation-symmetric problems can be reproduced using n extra qubits and a number of extra coupling terms of the form $\hat{\sigma}_z^{(j)} \hat{\sigma}_z^{(k)}$ which scales as n^2 , see Ref. [12]. It has also been suggested that adding a single additional qubit may allow such models to be fully realized perturbatively [26, 27]. Although this approach to construct such terms is much closer to the realm of what can be experimentally realized, it would still be highly non-trivial to implement. Nonetheless, the insights that can be gained from studying the search problem can be adapted to realistic problems of practical interest.

C. Adiabatic quantum search algorithm

Adiabatic quantum computing (AQC), first introduced by Farhi et al. [25], works as follows. The problem of interest is encoded into an n -qubit Hamiltonian \hat{H}_p in such a way that the solution can be derived from the ground state of \hat{H}_p . The system is initialized in the ground state of a different Hamiltonian \hat{H}_0 , for which this initialization is easy. The computation then proceeds by implementing a time-dependent Hamiltonian that is transformed slowly from \hat{H}_0 to \hat{H}_p . In general this adiabatic ‘sweep’ Hamiltonian can be parameterized in terms of a time-dependent schedule function $s \in [0, 1]$ as

$$\hat{H}_{\text{AQC}}(s) = (1-s)\hat{H}_0 + s\hat{H}_p, \quad (8)$$

with $s \equiv s(t/t_f)$ such that $s(0) = 0$ and at the final time t_f we have $s(1) = 1$. It is useful to define a reduced time $\tau = t/t_f$, with $0 \leq \tau \leq 1$. Whereas τ is linear in t , the schedule function $s(\tau)$ allows for nonlinear transformation. As we will see, nonlinear schedules are essential to obtain a quantum speed up.

The adiabatic theorem of quantum mechanics [28] says that the system will stay in the instantaneous ground state of the time-dependent Hamiltonian $\hat{H}_{\text{AQC}}(s)$ provided the following two conditions are satisfied: (i) there is at all times an energy gap $g(s) > 0$ between the instantaneous ground and first excited states, and (ii)

the Hamiltonian is changed sufficiently slowly. Provided these are both true the system will be in the desired ground state of \hat{H}_p at the end of the computation, thus solving the problem encoded in \hat{H}_p . In practice, the duration of this adiabatic sweep would be prohibitively long, so a feasible sweep will incur some probability of error. We discuss this and other subtleties of the adiabatic theorem in Sec. IID, after we introduce the adiabatic quantum search algorithm. For a comprehensive overview of AQC, see Albashi and Lidar [29].

Roland and Cerf [18] describe how adiabatic quantum computing can be used to solve the search problem. Defining our problem Hamiltonian as

$$\hat{H}_p = \hat{\mathbb{1}} - |m\rangle\langle m|, \quad (9)$$

whose non-degenerate ground state is equal to the marked state $|m\rangle$ with eigenvalue zero. We then need to choose our easy Hamiltonian \hat{H}_0 such that it has $|\psi_{\text{init}}\rangle$, as defined in Eq. (1), as its non-degenerate ground state. There are many possible choices, Roland and Cerf use $\hat{H}_0 = \hat{\mathbb{1}} - |\psi_{\text{init}}\rangle\langle\psi_{\text{init}}|$. With our system initialized in $|\psi_{\text{init}}\rangle$, we implement the time-dependent Hamiltonian in Eq. (8) with a suitable schedule function $s(\tau)$ so that the final state of the system is close to the marked state $|m\rangle$. Roland and Cerf demonstrate that a linear schedule function $s(\tau) = \tau = t/t_f$ does not produce a quantum speed up. It is necessary to use a more efficient nonlinear $s(\tau)$ whose rate of change is in proportion to the size of the gap $g(s)$ at that point in the schedule, in order to reproduce the quadratic speed up of Grover's search algorithm.

It is easy to show that $\hat{H}_0 = \hat{\mathbb{1}} - |\psi_{\text{init}}\rangle\langle\psi_{\text{init}}|$ is proportional to the adjacency operator of the fully-connected graph with $N = 2^n$ vertices. For the reasons already given in the context of the quantum walk search algorithm, a Hamiltonian corresponding to a less connected graph is preferable for practical applications. In order to make direct comparisons between adiabatic and quantum walk searching, we use the hypercube graph, with adjacency operator

$$\hat{H}_0^{(h)} = - \sum_{j=1}^n \hat{\sigma}_x^{(j)} \quad (10)$$

since this also has $|\psi_{\text{init}}\rangle$ as its non-degenerate ground state. Combining Eqs. (9) and (10), we have the adiabatic quantum computing Hamiltonian for search on a hypercube,

$$\hat{H}_{\text{AQC}}^{(h)} = (1-s) \left(- \sum_{j=1}^n \hat{\sigma}_x^{(j)} \right) + s (\mathbb{1} - |m\rangle\langle m|). \quad (11)$$

Noting that the identity term just shifts the zero point of the energy scale, we see that $\hat{H}_{\text{AQC}}^{(h)}$ contains the same terms as $\hat{H}_{\text{QWS}}^{(h)}$ in Eq. (6), only in different, time-varying proportions. It remains to specify the function $s(\tau)$ for

the optimal performance of this Hamiltonian for searching. There are several subtleties to deriving an optimal $s(\tau)$ that we address in the next subsection.

D. Optimising annealing schedules

As promised, we now return to the nuances of the adiabatic theorem and how, in the regime of limited running time, the schedule $s(\tau)$ may be optimized to minimize the error. A more quantitative statement of the adiabatic theorem [18, 25] proceeds as follows: Consider a time-dependent Hamiltonian of the form in Eq. (8), with initial and final Hamiltonians \hat{H}_0, \hat{H}_p respectively, and parameterized by the schedule function $s(\tau)$ that sweeps from $s(0) = 0$ to $s(1) = 1$ over a time t_f , the runtime of the sweep. Denote by $|E_j, t\rangle$ the j th energy eigenstate of the Hamiltonian at time t and its energy by $E_j(t)$, where $j = 0, 1$ denotes the ground and first excited states respectively. Provided that $E_2(t) > E_1(t)$ for $t \in [0, t_f]$ and transitions to higher energy eigenstates can be ignored, the final state obeys

$$|\langle \psi(t_f) | E_0, t_f \rangle|^2 \geq 1 - \epsilon^2, \quad (12)$$

provided that at all times

$$\frac{\left| \left\langle \frac{d\hat{H}}{dt} \right\rangle_{0,1} \right|}{g^2(t)} \leq \epsilon \ll 1, \quad (13)$$

where the matrix element $\langle d\hat{H}/dt \rangle_{0,1}$ and the gap $g(t)$ are given by

$$\left\langle \frac{d\hat{H}}{dt} \right\rangle_{0,1} = \left\langle E_0, t \left| \frac{d\hat{H}}{dt} \right| E_1, t \right\rangle \quad (14)$$

and

$$g(t) = E_1(t) - E_0(t). \quad (15)$$

However, adiabatic protocols derived from Eq. (13) are not always optimal. This equation is a condition on the instantaneous rate at which probability amplitude will leave the ground state for the first excited state, assuming the first excited state is not populated. Thus it does not apply where transfer directly to a higher excited state dominates over, or is competitive with, transfer to the first excited state, as such transitions are not taken into account. We can therefore describe Eq. (13) as a two-level approximation. In the context of the search algorithms studied here, such an approximation turns out to become more accurate for larger search spaces, and we make use of this in Sec. IV B.

Equation (13) also does not take into account the return of probability amplitude which has already entered the excited state. Such effects can become the most relevant to the dynamics under two circumstances. If the

first excited state is populated significantly, then non-adiabatic dynamics can occur such that this amplitude returns and interferes with the ground state amplitude. It is this regime which we primarily study in this work. Quantum walk dynamics are an extreme example of such behaviour as they can be viewed as coherent evolution bracketed by instantaneous quenches, which are the ultimate non-adiabatic transitions. The second and more subtle case is deep in the adiabatic regime, where the Hamiltonian sweep rate is so slow that the rate of excitation formation is very low during the middle of the anneal. In these cases, boundary effects which depend in a complicated way on both the nature of the annealing schedule and the total runtime t_f , become important [30, 31]. While this regime is very interesting, it is outside of the scope of our current study, and not relevant for practical implementation of algorithms. For this reason we limit our numerical studies to a maximum runtime of $4\pi/g_{\min}^2$, the square of the typical runtime derived from the minimum gap. With runtimes $t_f \lesssim 4\pi/g_{\min}^2$, we do not observe any appreciable boundary effects in our numerical results.

Roland and Cerf [18] derive a schedule $s(\tau)$ for the fully connected graph by optimizing Eq. (13). This schedule produces the full \sqrt{N} quantum speed up for the adiabatic quantum search algorithm. Following the method of Roland and Cerf [18] we can do an analogous calculation for the hypercube graph Hamiltonian given by Eq. (11). We fix $\langle d\hat{H}_{\text{AQC}}^{(h)}/dt \rangle_{0,1} = 1$, a good approximation that we will return to later, and solve the resulting adiabatic condition for the optimal schedule $s^{(o)}$ to give

$$s^{(o)} = \frac{1}{2\sqrt{N}} \tan \left[\frac{2\epsilon t}{\sqrt{N}} - \arctan(\sqrt{N}) \right] + \frac{1}{2} \quad (16)$$

for $N \gg 1$, with a runtime given by

$$t_f^{(o)} = \frac{\sqrt{N}}{\epsilon} \arctan(\sqrt{N}) \approx \frac{\pi}{2\epsilon} \sqrt{N}, \quad (17)$$

where the approximation becomes exact as $N \rightarrow \infty$.

However, as we demonstrate in Sec. IV C, for the modest values of N that we simulate, this schedule $s^{(o)}$ does not provide the optimal \sqrt{N} scaling. We need to include a correction term to the above approximation, to take into account the point at which the minimum gap occurs. The relevant calculation of the eigensystem is given in Refs. [21, 25] in the context of quantum walk searching. Using these results, we find a corrected schedule

$$s^{(c)} = \frac{1}{2\sqrt{N}} \tan \left[\frac{2\epsilon t}{\sqrt{N}} - \arctan(2c\sqrt{N}) \right] + c, \quad (18)$$

with runtime given by

$$t_f^{(c)} = \frac{\sqrt{N}}{2\epsilon} \left\{ \arctan[2c\sqrt{N}] + \arctan[2(1-c)\sqrt{N}] \right\}, \quad (19)$$

where the correction c is given by

$$c = \frac{2^{n+1}}{n \sum_{r=1}^n \binom{n}{r} \frac{1}{r} + 2^{n+1}}. \quad (20)$$

We demonstrate in Sec. IV C that $s^{(c)}$ is able produce an optimal \sqrt{N} speed up for quantum searching. Notice that we can also express $s^{(c)}$ in terms of the optimal quantum walk step rate $\gamma_h^{(o)}$ for the hypercube graph in Eq. (7), using

$$c = \frac{1}{1 + \gamma_h^{(o)}}. \quad (21)$$

Instead of estimating the gap based on a two level approximation, we can solve Eq. (13) numerically to obtain $s^{(n)}$ with explicit calculation of g as a function of t , using the algorithm we describe in Sec. III B. Crucially, this method still assumes $\langle d\hat{H}_{\text{AQC}}^{(h)}/dt \rangle_{0,1} = 1$, so still relies on a variant of the two level approximation. While this does not provide a closed form solution, results using $s^{(n)}$ do provide insight on the accuracy of $s^{(c)}$. Provided the numerics are performed to a sufficient accuracy, $s^{(n)}$ will always provide an optimal \sqrt{N} speed up.

However, note that all of these schedules assume a two-level approximation, as they start from Eq. (13). In Sec. IV C we give an example of how this limitation can lead to a regime where $s^{(c)}$ performs slightly better than $s^{(n)}$, and discuss how this arises from a partial cancellation of errors in $s^{(c)}$ from (i) the breakdown of the two-level approximation and (ii) the breakdown of the approximation $\langle d\hat{H}_{\text{AQC}}^{(h)}/dt \rangle_{0,1} = 1$.

III. GENERALIZED ANNEALING SCHEDULES

A. Motivation and derivation

We have already noted that quantum walk and adiabatic quantum computing search algorithms can both use the same terms in the Hamiltonian, differing only in the time dependence. With appropriate choice of parameters, both provide a quadratic quantum speed up, a search time proportional to \sqrt{N} for a search space of size N . What we want to find out is, can we map smoothly from QW to AQC searching, while maintaining the quantum speed up?

To do the mapping, we generalize the AQC Hamiltonian of Eq. (8) by defining a time-dependent Hamiltonian

$$\hat{H}(\tau) = A(\tau)\hat{H}_0 + B(\tau)\hat{H}_p \quad (22)$$

as a function of the reduced time $\tau = t/t_f$, where the annealing schedules $A(\tau)$, $B(\tau)$ satisfy $A(0) \gg B(0)$ and $B(1) \gg A(1)$. The AQC algorithm as described by Eq. (8) is obtained by setting

$$\begin{aligned} A_{\text{AQC}}(\tau) &= 1 - s(\tau) \\ B_{\text{AQC}}(\tau) &= s(\tau). \end{aligned} \quad (23)$$

The QW search Hamiltonian described by Eq. (6) can also be described (up to an irrelevant term proportional to the identity) by setting

$$\begin{aligned} A_{\text{QW}}^{(\gamma)}(\tau) &= \begin{cases} \gamma & \tau < 1 \\ 0 & \tau = 1 \end{cases} \\ B_{\text{QW}}^{(\gamma)}(\tau) &= \begin{cases} 1 & \tau > 0 \\ 0 & \tau = 0. \end{cases} \end{aligned} \quad (24)$$

We can make this even closer to the AQC form by defining $\beta = 1/(1 + \gamma)$ and setting

$$\begin{aligned} A_{\text{QW}}(\tau) &= \begin{cases} 1 - \beta & \tau < 1 \\ 0 & \tau = 1 \end{cases} \\ B_{\text{QW}}(\tau) &= \begin{cases} \beta & \tau > 0 \\ 0 & \tau = 0. \end{cases} \end{aligned} \quad (25)$$

Using Eq. (7) for $\gamma_h^{(o)}$, to achieve optimal \sqrt{N} scaling for a quantum walk search, we must set

$$\beta = \beta_h^{(o)} = c = \frac{2^{n+1}}{n \sum_{r=1}^n \binom{n}{r} \frac{1}{r} + 2^{n+1}}, \quad (26)$$

where we note from Eq. (20) that $c \equiv \beta_h^{(o)}$.

For $0 < \tau < 1$, the re-parameterization of Eq. (24) in Eq. (25) maintains the ratio of $A_{\text{QW}}(\tau)/B_{\text{QW}}(\tau) = \gamma$. However, it also introduces a global energy shift $A_{\text{QW}}(\tau) = \beta A_{\text{QW}}^{(\gamma)}(\tau)$ and $B_{\text{QW}}(\tau) = \beta B_{\text{QW}}^{(\gamma)}(\tau)$. The observant reader will note that, because the optimal $\gamma_h^{(o)}$ is dependent on the size of the system, this re-parameterization introduces a weak dependence of the global energy scale on system size $N = 2^n$. However, since $\beta_h^{(o)} \rightarrow \frac{1}{2}$ in the large N limit, this weak dependence cannot affect the leading order term in the asymptotic scaling, and the re-parameterized quantum walk search algorithm still provides optimal \sqrt{N} scaling.

In the way we have parameterized them above, the AQC and QW protocols differ only in the annealing schedules $A(\tau)$ and $B(\tau)$. Hence, we can use the QW and AQC schedules as end-points of a smooth interpolation between these two search algorithms to define a continuum of hybrid protocols. Using a parameter $\alpha \in [0, 1]$, where $\alpha = 0$ corresponds to QW and $\alpha = 1$ corresponds to AQC, we can define

$$\begin{aligned} A(\alpha, \beta, \tau) &= \frac{1 - s(\tau)}{\alpha + (1 - \alpha) \frac{(1 - s(\tau))}{(1 - \beta)}} \\ B(\alpha, \beta, \tau) &= \frac{s(\tau)}{\alpha + (1 - \alpha) \frac{s(\tau)}{\beta}}. \end{aligned} \quad (27)$$

giving a family of hybrid quantum search algorithms on the hypercube defined by the Hamiltonian

$$\hat{H}_{\text{AB}}^{(h)} = A(\alpha, \beta, \tau)\hat{H}_0^{(h)} + B(\alpha, \beta, \tau)(\mathbb{1} - |m\rangle\langle m|) \quad (28)$$

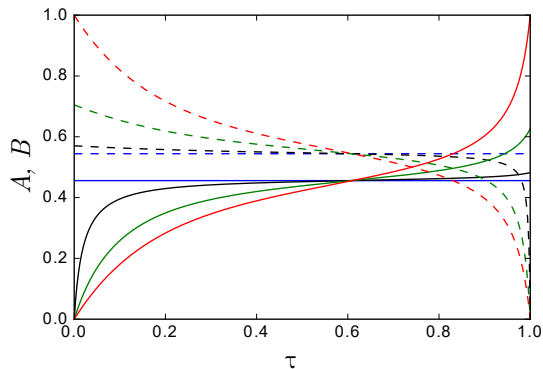


FIG. 1. (color online) Interpolated schedule functions $A(\alpha, \beta, \tau)$ (dashed lines) and $B(\alpha, \beta, \tau)$ (solid lines) as defined by Eq. (27) for hybrid QW-AQC quantum searching on an $n = 5$ dimensional hypercube graph, QW, $\alpha = 0$, blue (dark gray in print); $\alpha = 0.1$, black; $\alpha = 0.5$, green (mid gray in print); and AQC, $\alpha = 1$, red (light gray in print), calculated numerically following the method in Sec. III B.

The resulting family of functions is illustrated in Fig. 1 for a search over a 5-qubit hypercube graph, $N = 2^5$.

To draw a fair comparison between AQC and QW performance, we must use an AQC schedule $s(\tau)$ for which the avoided crossing position (the point where ds/dt is minimal) is equal to β . Otherwise, such a comparison may be more of a measure of which of these points has been chosen more appropriately than the performance of the underlying mechanisms. Hence, we choose $\beta = 1/2$ for interpolations involving the unshifted two level approximation $s^{(o)}$, and the true optimal value of $\beta_n^{(o)}$ for both the corrected two level approximation $s^{(c)}$ and the numerically calculated optimal schedule $s^{(n)}$.

Note that it doesn't follow *a priori* from the construction that these interpolated AQC-QW schedules will yield a quantum speed up at all, let alone an optimal \sqrt{N} scaling. We return to this important question in Sec. IV, where we show that properly constructed interpolations can indeed achieve the theoretical optimum \sqrt{N} scaling.

B. Numerical methods

Our small system examples have been simulated using the full Hamiltonian on the hypercube. To examine how our hybrid quantum search algorithms scale, we can take advantage of the extreme symmetry of the hypercube to map the dynamics to a search on the line with appropriately weighted edges. This allows us to perform simulations for much larger numbers of qubits n , and hence extract reliable information about the scaling with n .

To map the hypercube search Hamiltonian to a line, we first apply a gauge transformation (a swap of the $1 \leftrightarrow 0$ labels on a subset of the qubits) to map the marked state to the state $|000\dots\rangle$. The marked state Hamiltonian is

now $\hat{H}_p^{\text{line}} = \hat{\mathbb{1}} - |0\rangle\langle 0|$, which is invariant under arbitrary permutations of the qubits. The hypercube Hamiltonian $\hat{H}_0^{(h)}$ is already invariant under such permutations (re-labeling of qubits) in any gauge (choice of which states are labeled 1 versus 0 for each qubit). Provided the initial state is also invariant with respect such permutations, the evolution will be restricted to the $n + 1$ states $|\psi(j, n)\rangle$ which preserve this symmetry. Such states can be written, up to normalization, as

$$|\psi(j, n)\rangle = \sum_{a_j \in \{q_j\}} \left(\prod_{k \in a_j} \hat{\sigma}_x^{(k)} \right) |00\dots\rangle + \delta_{j=0} |00\dots\rangle, \quad (29)$$

where $\{q_j\}$ is the set of all states where j of the n total bits are 1. Within this restricted subspace, the matrix elements of the hypercube Hamiltonian \hat{H}_0^{line} become

$$\begin{aligned} (\hat{H}_0^{\text{line}})_{j,k} &= - \left\langle \psi(j, n) \left| \sum_{l=1}^n \hat{\sigma}_x^{(l)} \right| \psi(k, n) \right\rangle \\ &= -2 \delta_{j-k=\pm 1} \sqrt{\mathfrak{s}(\mathfrak{s} + 1) - m_{\mathfrak{s}}(m_{\mathfrak{s}} \pm 1)}, \quad (30) \end{aligned}$$

which is effectively the Hamiltonian of a single spin n object with $\mathfrak{s} = \frac{n}{2}$ and $m_{\mathfrak{s}} = \frac{1}{2} \min(k, j)$. This Hamiltonian has been studied extensively, for details in the context of quantum search algorithms, see Child and Goldstone [21].

Combined with the marked state Hamiltonian \hat{H}_p^{line} , we have our full Hamiltonian for the search mapped to the line

$$\hat{H}^{\text{line}}(\tau) = A(\alpha, \beta, \tau) \hat{H}_0^{\text{line}} + B(\alpha, \beta, \tau) \hat{H}_p^{\text{line}}, \quad (31)$$

for any hybrid protocol defined by $A(\alpha, \beta, \tau)$ and $B(\alpha, \beta, \tau)$ and chosen schedule $s(\tau)$.

Our numerical calculations were carried out using the Python programming language (both Python 2.7 and Python 3.5), making considerable use of the NumPy, SciPy and Matplotlib packages [32–36]. High performance computing resources were not used in this study, although some of the simulations took several days to run on standard desktop workstations. Most of the simulations consisted of solving the time evolution of the quantum search algorithm by numerically integrating the Schrödinger equation using the appropriate Hamiltonian, by diagonalising the Hamiltonian and exponentiating it in the diagonal basis, before applying it to the wave function. This process was iterated for time dependent Hamiltonians, rotating from one instantaneous diagonal basis to the next at small time intervals. For the decoherence studies in Sec. V C, the same process was applied to the density matrix, with dephasing operators also applied along with the unitary time evolution.

Optimal AQC schedules $s^{(n)}(\tau)$ were calculated numerically, due to the difficulty of finding exact analytical solutions for the hypercube. Based on the arguments in [18], we know that an AQC schedule which is optimal under a set of approximations can be found by solving $|\frac{ds}{dt}| = \epsilon g^2(s)$. We demonstrate in Sec. IV C that

schedules calculated in this way are actually not the optimal AQC schedules for the hypercube, because some of the approximations of [18] are not satisfied. For the hypercube, the matrix which describes these systems is $(n+1) \times (n+1)$, even after taking advantage of symmetry by mapping to a line. A Hermitian 2×2 matrix can always be diagonalized analytically by finding the roots of the characteristic polynomial, as was done in [18]. For larger matrices this is no longer feasible, nor generally possible if the matrix is bigger than 4×4 . Fortunately, the gap $g(s)$ can easily be calculated numerically, and we are thence able to iteratively solve $|\frac{ds}{dt}| = \epsilon g^2(s)$. We first define a normalized function

$$F(s) = \int_0^s ds' \frac{1}{\epsilon g^2(s')} \times \left[\int_0^1 ds' \frac{1}{\epsilon g^2(s')} \right]^{-1}, \quad (32)$$

where s is a function of the reduced time τ . To obtain $s(\tau)$, we need to invert this function, $s(\tau) = F^{-1}(\tau)$.

Deliberately using a programming-like notation, we define τ LIST to be a linearly spaced list of points between $\tau = 0$ and $\tau = 1$, and s LIST to be a list of the corresponding values of $s(\tau)$, obtained by applying $F^{-1}(\tau)$ to each element of τ LIST. We approximate $F(s)$ numerically by $\tilde{F}(s)$, where we replace the integral by a finite sum plus linear interpolation. Writing $\tilde{s}_j = \frac{1}{2}(s\text{LIST}(j(s)) + s\text{LIST}(j(s) + 1))$

$$\begin{aligned} \tilde{F}(s) &= \sum_{j'=1}^{j(s)} \frac{s\text{LIST}(j'+1) - s\text{LIST}(j')}{\mathcal{N} g^2(\tilde{s}_{j'})} \\ &+ \frac{s - s\text{LIST}(j(s))}{\mathcal{N} g^2(\tilde{s}_j)}, \end{aligned} \quad (33)$$

where $j(s)$ is equal to the number of elements in s LIST which are strictly less than s , and \mathcal{N} is a normalization factor which is included to ensure that $\hat{F}(s) = 1$. It is straightforward to numerically invert $\hat{F}(s)$. This can be accomplished by first finding $j_{\max}(s)$, the largest value of $j(s)$ for which $\hat{F}(s) < \tau$, and then solving

$$\hat{F}(s)|_{j(s)=j_{\max}(s)} = \tau \quad (34)$$

for s . Based on this numerical function inversion, we define an iterative method of converging on the solution for $s^{(n)}(\tau)$,

1. set a linearly spaced s LIST $\in [0, 1]$ and τ LIST $\in [0, 1]$ each with the same number of elements
2. using the values of s in s LIST, apply $\hat{F}^{-1}(\tau)$ to each corresponding element in τ LIST to generate a new s LIST
3. repeat step 2. with the new s LIST as input, until it has converged

The advantage of this iterative method is that, at each iteration, more points in s LIST will concentrate in areas where $1/g^2$ is larger, for instance near the dominant avoided crossing. By using the previously calculated

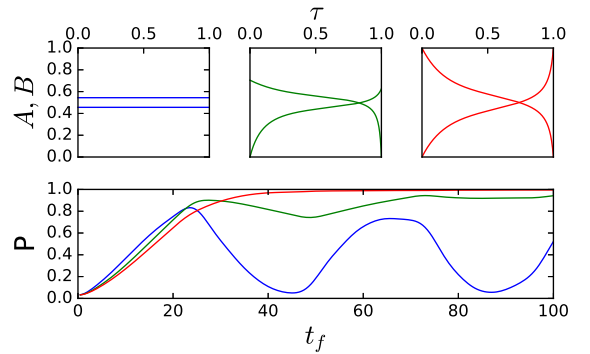


FIG. 2. (color online) (Top) Numerically calculated hybrid schedules A and B against reduced time τ for quantum search on a 5-qubit hypercube graph for $\alpha = 0$ QW, blue (dark gray in print, top left), $\alpha = 0.5$ green (mid gray in print, top middle), and $\alpha = 1$ AQC, red (light gray in print, top right). (Bottom) Success probability of the corresponding searches (indicated by matching colour/shade of gray in print) against total search time t_f .

s LIST as a mesh in the current iteration, the protocol can continuously improve the quality of the numerical inverse with a fixed number of points in s LIST.

C. Small system examples

Before presenting our main results on hybrid quantum searches, we examine the behavior of interpolated schedules for small systems of five and eight qubits. These results provide the first evidence for how the AQC and QW mechanisms interact. Fig. 2 shows how the final success probability varies with the search duration t_f for QW, AQC and an intermediate $\alpha = 0.5$ search over the 5-qubit hypercube graph. Note that, because the schedules A and B are in general nonlinear functions of time, in all plots against t_f each point represents a separate run of the quantum search algorithm for that value of t_f ; the plots do not also represent the time evolution $0 \leq t \leq t_f$, except for $\alpha = 0$ when the schedule functions are constant ($A = 1 - \beta$ and $B = \beta$). Also plotted in Fig. 2 are the annealing schedules A and B as a function of the reduced time τ , illustrating how the shape of the functions $A(\alpha, \tau)$ and $B(\alpha, \tau)$ changes for different values of α , from flat for a quantum walk to a curving AQC annealing schedule for $\alpha = 1$. We see that the qualitative behaviour of adiabatic evolution is fundamentally different from that of the quantum walk search. For the optimal AQC schedule the success probability increases monotonically to a value very close to one. In contrast, QW shows oscillatory behaviour, and although the success probability does not approach one, it does show a faster initial increase than for AQC. The intermediate schedule shows a mix of both behaviours, with a locally oscillating but globally increasing success probability that shows an initial increase rate

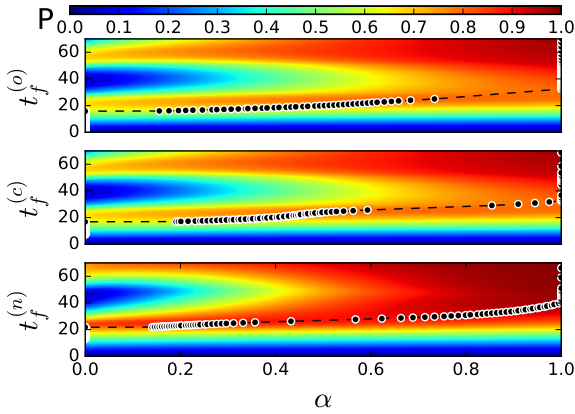


FIG. 3. (color online) Success probabilities P of hybrid QW-AQC quantum search on a 5-qubit hypercube graph plotted against the interpolation parameter α and total runtime t_f using (top) schedule $s^{(o)}$ derived from a simple two-level approximation, Eq. (16), (middle) $s^{(c)}$ from two-level approximation with crossing-point correction given by Eq. (18), and (bottom) $s^{(n)}$ from numerical solution. Dotted lines with black points indicate the optimal protocol at a given runtime t_f .

between that of QW and AQC.

We now turn to the probability P of finding the marked state that is obtained for different choices of α and t_f . For all allowed strategies across a continuum of α values, Figs. 3 and 4 illustrate the same qualitative behaviour for 5-qubit and 8-qubit quantum searches. The oscillatory behaviour associated with a QW slowly fades away as the interpolation approaches the respective AQC schedule, at which point the success probability P increases monotonically with t_f . If a low success probability is required, only a short total runtime t_f is necessary, and quantum walk is the best strategy. As t_f is increased, the best strategy is to increase α and start adding some adiabatic character into the protocol. Finally, if a high success probability is required after a long runtime t_f , then whichever optimal AQC schedule is being used becomes the best strategy. We also see that, for these system sizes and the better optimal schedules $s^{(c)}$ and $s^{(n)}$, the hybrid protocols maintain the quantum speed up for the search algorithm runtime.

We now examine the differences between the three annealing strategies $s^{(o)}$, $s^{(c)}$ and $s^{(n)}$ on these small systems. Fig. 3 depicts results for $n = 5$ qubits. The main difference for five qubits is that the numerically calculated optimal schedule $s^{(n)}$ is able to perform substantially better than the other two, where “better” means a higher probability of success for a given runtime t_f and value of α . Figure 4 shows the same comparisons for the slightly larger value of $n = 8$ qubits. The shifted two level approximation $s^{(c)}$ and numerically optimized schedule $s^{(n)}$ are now quite similar, while the simple two level approximation $s^{(o)}$ performs poorly with lower success probabilities. It also exhibits a faster oscillation frequency for the quantum walk, which is indicative of be-

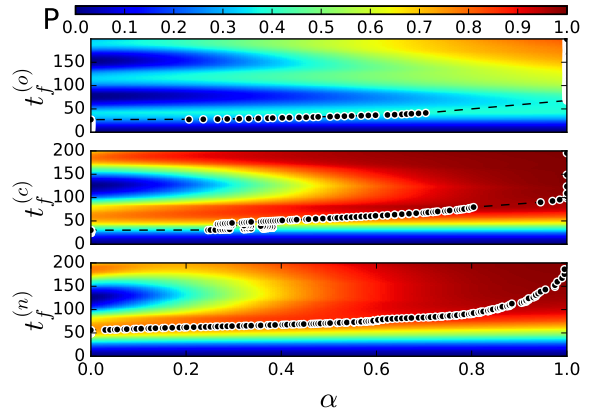


FIG. 4. (color online) Success probabilities P of hybrid QW-AQC quantum search on an 8-qubit hypercube graph plotted against the interpolation parameter α and total runtime t_f using (top) schedule $s^{(o)}$ derived from a simple two-level approximation, Eq. (16), (middle) $s^{(c)}$ from two-level approximation with crossing-point correction given by Eq. (18), and (bottom) $s^{(n)}$ from numerical solution. Dotted lines with black points indicate the optimal protocol at a given runtime t_f .

ing away from the avoided crossing due to a sub-optimal value of γ . The optimal α moves away from $\alpha = 0$ at a smaller value of t_f and P for $s^{(c)}$ than it does for $s^{(n)}$. There is also more structure in the optimal α line (black dashes) for $s^{(c)}$ than for $s^{(n)}$. Otherwise, the two behave quite similarly for these small sizes, suggesting that both $s^{(c)}$ and $s^{(n)}$ are able to provide a quantum speed up for hybrid protocols. To confirm this in general, not just for small n , further analysis and simulations of larger systems are required, which we tackle in the next section.

IV. PERFORMANCE OF HYBRID ALGORITHMS

A. Minimum gap scaling

For all protocols, the Hamiltonian is similar around the position of the lowest avoided energy level crossing between E_0 and E_1 . Our strategy for analyzing the scaling of the hybrid algorithms is to show that the performance is dominated by this avoided crossing, which is present at the same position in all hybrid algorithms. We then analyze the scaling of the avoided crossing in detail. We show that hybrid algorithms do not bring in any extra features that affect the scaling, in other words, that the scaling is determined by the behavior at the minimum gap, which is independent of the interpolation parameter α . The behavior does depend on β and $s(\tau)$, which must be correctly specified to obtain a quantum speed up. For an optimal schedule, the minimum gap occurs where $B(\alpha, \beta, \tau) = s(\tau) = \beta$ and $ds(\tau)/dt$ takes its minimum value.

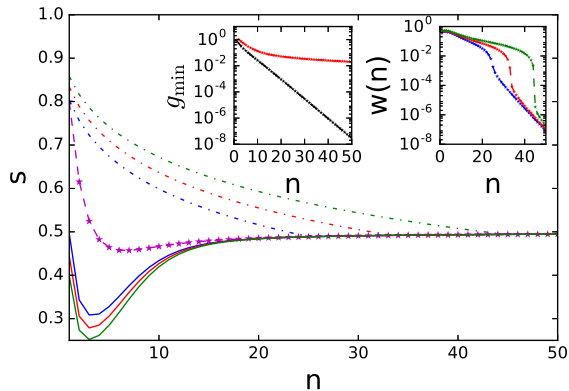


FIG. 5. (color online) Main figure: $s(\tau)$ against number of qubits n for 90% (blue, dark gray in print), 93% (red, light gray in print), 95% (green, mid gray in print) overlap of $|\psi(t)\rangle$ with $|m\rangle$ (solid) and with $|\psi_{\text{init}}\rangle$ (dot-dashed). Magenta stars are the transition point, the value of $s(\tau)$ when the minimum gap g_{min} occurs. Left inset: $g_{\text{min}} = \min(E_1 - E_0)$ (lower black stars) and $\min(E_2 - E_0)$ (upper red stars, light gray in print). Right inset: width of the transition $w(n) = \Delta s(\tau)$, the difference between solid and dot-dashed curves of the same color in the main figure. Calculated using the hypercube QW mapped to the line.

To show numerically that the avoided crossing is the only relevant feature in the large N limit, we must demonstrate two things. First, that the minimum gap $g_{\text{min}} = (E_1 - E_0)$ between the ground state and the first excited state becomes much smaller than the minimum gap between the ground state and the second excited state. Second, that the lowest avoided level crossing, where $g(\tau) = g_{\text{min}}$, dominates the transition between the ground state of the hypercube Hamiltonian $\hat{H}_0^{(h)}$ and the ground state of the marked state Hamiltonian \hat{H}_p , and becomes more dominant as system size increases. Figure 5 shows that both of these do, in fact, occur. The left inset shows that at the avoided crossing, the gap between the ground state and first excited state shrinks exponentially faster in n than the gap between the ground state and second excited state. The main figure and right inset of Fig. 5 show how the transition between the two ground states becomes dominated by the dynamics at g_{min} as n increases.

For a pure quantum walk search, this convergence to behaviour dominated by a single avoided crossing can be seen in Fig. 6, which shows that not only does the search success probability P approach one in the large system limit (main figure), but also that the time evolution of P (inset) approaches the functional form for the single avoided crossing $P(\tau) = \sin^2(\tau g_{\text{min}})$. The non sinusoidal shapes of these curves at low qubit number are due to the influence of excited states higher than the first excited state. In the main figure, these small size effects are clearly significant up to about $n = 12$ qubits. Thereafter, P approaches one smoothly although relatively slowly as a function of n .

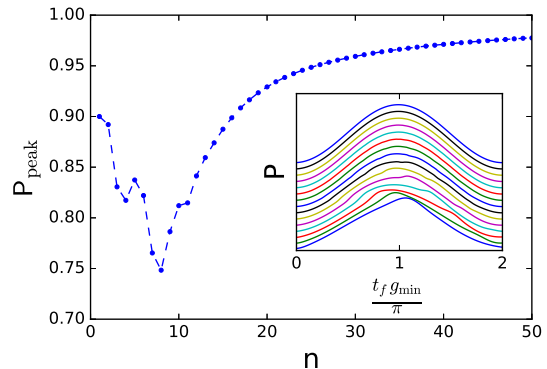


FIG. 6. (color online) Main figure: Search success probability P at the first peak for a quantum walk search against qubit number n up to $n = 50$. Inset: Rescaled offset plot of P against t starting at the bottom with $n = 5$ qubits and going to $n = 20$. Calculated using the hypercube QW mapped to the line.

Since states of higher energy than the first excited state play very little role in the QW search dynamics for larger systems, we can approximate the probability that the marked state can be reached by considering only the ground and first excited states. Starting in $|\psi_{\text{init}}\rangle$, the probability of evolving to the ground state $|E_0\rangle$ or first excited state $|E_1\rangle$ of the full search Hamiltonian $\hat{H}_{\text{QWS}}^{(h)}$, and then to the marked state $|m\rangle$, is given by the product of the sums of the overlaps,

$$P_{\text{max}}^{(QW)} = (|\langle \psi_{\text{init}} | E_0 \rangle|^2 + |\langle \psi_{\text{init}} | E_1 \rangle|^2) \times (|\langle E_0 | m \rangle|^2 + |\langle E_1 | m \rangle|^2), \quad (35)$$

when higher energy levels are neglected.

Figure 7 shows how $P_{\text{max}}^{(QW)}$ approaches one as n increases, by plotting the difference from one on a log or log-log scale. The top left figure shows that $P_{\text{max}}^{(QW)} \rightarrow 1$ only happens relatively slowly, with a polynomial scaling in n , and therefore logarithmic in N . By plotting the two overlaps in Eq. (35) separately, the left figure shows that the overlap of $|\psi_{\text{init}}\rangle$ with $|E_0\rangle$ and $|E_1\rangle$ rapidly approaches one. The top right figure shows that the scaling of $P_{\text{max}}^{(QW)}$ is dominated by the overlap of the marked state with the lowest energy states $|E_0\rangle$ and $|E_1\rangle$ at the gap. We can quantify how slowly P approaches one by doing numerical fits to determine the scaling of the relevant quantities: these are summarized in table I. In particular, we note that $\gamma_h^{(o)}$ only approaches one linearly in n , consistent with the analytical results in Ref. [21]. We show in the next section that this slow approach leads to a failure of schedules with $s = s^{(o)}$ and $\beta = \frac{1}{2}$ to obtain a quantum speed up for all values of α . The fact that $P_{\text{max}}^{(QW)} \rightarrow 1$ suggests that the optimal protocol for all success probabilities should approach QW ($\alpha = 0$) for large system size, because QW does not slow down at the

Quantity	Scaling	$1 - r^2$
$P_{\max}^{(QWS)}$	$1 - 1.734 \times n^{-1.112}$	7.820×10^{-5}
$ \langle E_0 m \rangle ^2 + \langle E_1 m \rangle ^2$	$1 - 1.734 \times n^{-1.112}$	7.820×10^{-5}
$ \langle \psi_{\text{init}} E_0 \rangle ^2 + \langle \psi_{\text{init}} E_1 \rangle ^2$	$1 - 4.292 \times 2^{-1.186 n}$	0.00143
$\gamma_h^{(o)}$	$1 - 1.233 \times n^{-1.0425}$	1.120×10^{-5}

TABLE I. Numerical fits for various quantities related to quantum walks and adiabatic protocols. These fits were performed using linear fitting on either logarithmic or semi-logarithmic axes in the range $n = 40$ to $n = 70$, except for $|\langle \psi_{\text{init}}|E_0 \rangle|^2 + |\langle \psi_{\text{init}}|E_1 \rangle|^2$ which was fit over the range $n = 11$ to $n = 40$ due to numerical precision issues. The coefficient of determination $r^2 \equiv 1 - \frac{\sum_i (y_i - f_i)^2}{\sum_i (y_i - \bar{y})^2}$, where f_i are the data and y is the fitting function, this coefficient is calculated against the linear function on the logarithmic or semi-logarithmic axes. These fits are plotted along with the data used to produce them in Fig. 7. The slight difference from -1 in the scaling exponent for γ_{opt} is due to numerical finite size effects.

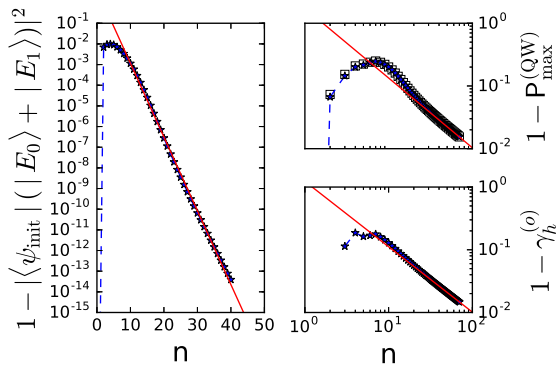


FIG. 7. (color online) Scaling of various quantities related to QW searching. Left: difference from one of the overlap of $|\psi_{\text{init}}\rangle$ with $|E_0\rangle$ and $|E_1\rangle$ against number of qubits n . Top Right: difference from one of marked state with $|E_0\rangle$ and $|E_1\rangle$ (stars) and $P_{\max}^{(QWS)}$ (squares), against n . Bottom right $1 - \gamma_h^{(o)}$ versus n . Solid lines (red online) are numerical fits, summarized in table I. Calculated using the hypercube QW mapped to the line.

minimum gap like AQC does. However, $P_{\max}^{(QW)} \rightarrow 1$ only happens relatively slowly: the maximum $P_{\max}^{(QW)}$ which a QW search obtains only reaches 99% by around 100 qubits. Brute force classical techniques will become computationally non-trivial beyond around 30 bits, where $P_{\max}^{(QW)} \approx 95\%$. The finite size effects we study here are thus relevant to real world applications.

As Fig. 8 illustrates, the optimal protocol does in fact become more quantum walk like as the system grows, both in terms of the search success probability at which QW is no longer the optimal strategy, and in terms of the α values of the optimal protocol once this has happened. Quantum walk becomes unfavorable as the optimal single run strategy when $P \approx P_{\max}^{(QW)}$, after which the hybrid strategies require runtimes t_f larger than g_{\min}/π to achieve higher success probabilities in a single run. We consider multiple run strategies in Sec. V, after we take a closer look at the scaling of a single run.

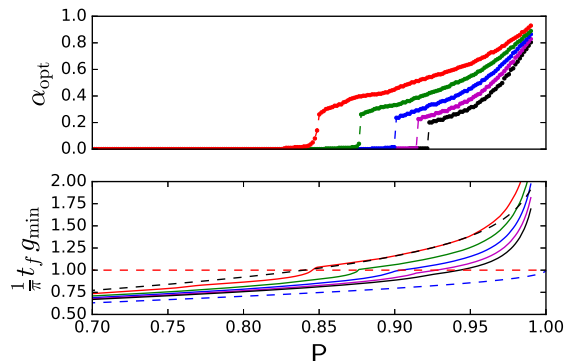


FIG. 8. (color online) Top: Value of interpolation parameter α giving the shortest runtime for a fixed success probability P for a single search, using numerically calculated optimal schedules $s^{(n)}$ for hypercube dimension $n = 12$ (red); $n = 14$ (green); $n = 16$ (blue); $n = 18$ (magenta); $n = 20$ (black). Bottom: Normalized runtime versus P for corresponding α and hypercube dimension as above (solid lines). Dashed lines: single avoided crossing model (large N limit) for $t_f = g_{\min}/\pi$, the time at which a QW reaches a success probability of one (red), time for QW to reach P (blue), time for AQC to reach P (black).

B. Single avoided crossing model

As Fig. 5 illustrates, the width $w(n)$ of the avoided crossing decreases rapidly with n . Even for a modest size of $n = 50$ qubits, the switch from 95% overlap with the hypercube Hamiltonian ground state to 95% overlap with the marked state occurs in less than 10^{-6} of the total dynamic range of the protocol, which runs from $s(\tau) = 0$ to $s(\tau) = 1$. A single avoided crossing dominates in the large N limit of a range of quantum search algorithms including search based on a hypercube, and therefore a single avoided crossing model is worth examining despite its extreme simplicity. Dominance of a single avoided crossing has been shown to be the typical behavior for a broad class of random search graphs [22]. Such behavior can also be seen more trivially for the fully connected graph, where symmetry causes the entire dynamics to be restricted to two energy levels, and it is also applicable to

searches on Cartesian lattices, which provide a quantum speed up for $d \geq 4$ dimensions [21].

The Hamiltonian of an avoided level crossing can conveniently be written as

$$\hat{H}_{\text{ac}}(\tilde{\tau}) = \mathcal{A}[-\hat{\sigma}_x + f(\tilde{\tau})\hat{\sigma}_z], \quad (36)$$

where $\tilde{\tau} = \tilde{t}/\tilde{t}_f$ is a rescaled reduced time parameter determined by the mapping from the original problem. The Hamiltonian $\hat{H}_{\text{ac}}(\tilde{\tau})$ is defined in the $(|\psi_{\text{init}}\rangle, |m\rangle)$ basis. By choosing this basis, we are implicitly assuming that these two states are orthogonal to a good approximation. Given that this model is used in the large N limit and $|\langle\psi_{\text{init}}|m\rangle|^2 \propto \frac{1}{N}$, this assumption is justified and becomes exact as $N \rightarrow \infty$. The parameter \mathcal{A} determine the energy scale of the minimum gap, which in turn depends on the specific details of the problem. In particular, the scaling of \mathcal{A} determines the scaling of the problem hardness. In this rescaled picture, we assume that very rapidly (relative to the time spent at the crossing) quenching through all parts of the annealing schedule not in the vicinity of the avoided crossing will not be detrimental to the quality of the solution, and therefore the avoided crossing can be treated as the only feature. We initialize at $\tilde{\tau} = 0$ with the state $|\psi_{\text{init}}\rangle$ as the ground state, pass through the avoided crossing at $\tilde{\tau} = \frac{1}{2}$, and end at $\tilde{\tau} = 1$ with the marked state $|m\rangle$ as the ground state. We therefore choose the boundary conditions such that $f(0) = -\infty$ and $f(1) = \infty$. This can be intuitively thought of as scaling all features of $\hat{H}_{\text{ac}}(\tilde{\tau})$ other than the avoided crossing to $\pm\infty$.

Having set up our general single avoided crossing model, we now map our hybrid quantum search algorithms on the hypercube, as defined in Eq. (27), onto this model. This allows us to determine the specific functional forms of $\tilde{\tau}$ and $f(\tilde{\tau})$ for hybrid search on a hypercube, and hence determine the runtime scaling of the hybrid algorithms. We first match the size of the minimum gap g_{min} in $\hat{H}_{\text{AB}}^{(h)}$ to the size of the minimum gap \tilde{g}_{min} in $\hat{H}_{\text{ac}}(\tilde{\tau})$, from which we find that $\mathcal{A} = g_{\text{min}}/2$. Assuming that $A(\alpha, \beta, \tau)$ and $B(\alpha, \beta, \tau)$ are continuous around the avoided level crossing, we perform a first order Taylor expansion about the avoided crossing at $s(\tau) = s_{\text{ac}}$. By applying second order perturbation theory, we find

$$\left. \frac{d^2 g(\tau)}{ds^2} \right|_{s=s_{\text{ac}}} = \frac{1}{2g_{\text{min}}} \left(\left. \frac{dA}{ds} \right|_{s=s_{\text{ac}}} - \left. \frac{dB}{ds} \right|_{s=s_{\text{ac}}} \right)^2. \quad (37)$$

Performing the same procedure for the single avoided crossing model of Eq. (36) yields

$$\left. \frac{d^2 \tilde{g}}{d\tilde{\tau}^2} \right|_{\tilde{\tau}=\frac{1}{2}} = \frac{1}{4} \left(\left. \frac{df}{d\tilde{\tau}} \right|_{\tilde{\tau}=\frac{1}{2}} \right)^2, \quad (38)$$

where $\tilde{g}(\tilde{\tau})$ is the rescaled gap. Note that, because $\tilde{\tau}$ only appears in Eq. (36) as an argument of $f(\tilde{\tau})$, there is an arbitrary scaling factor a such that $\tilde{\tau} \rightarrow a\tilde{\tau}$ gives

$f(\tilde{\tau}) \rightarrow f(\tilde{\tau}/a)$. We therefore set

$$\left. \frac{d^2 g}{ds^2} \right|_{s=s_{\text{ac}}} = \lambda \left. \frac{d^2 \tilde{g}}{d\tilde{\tau}^2} \right|_{\tilde{\tau}=\frac{1}{2}}, \quad (39)$$

where the proportionality factor $\lambda > 0$ determines the arbitrary scaling factor a . The relationship between $f(\tilde{\tau})$ and $A(\alpha, \beta, \tau)$ and $B(\alpha, \beta, \tau)$ thus satisfies

$$\left. \frac{df}{d\tilde{\tau}} \right|_{\tilde{\tau}=\frac{1}{2}} = \sqrt{\frac{2\lambda}{g_{\text{min}}}} \left(\left. \frac{dB}{ds} \right|_{s=s_{\text{ac}}} - \left. \frac{dA}{ds} \right|_{s=s_{\text{ac}}} \right). \quad (40)$$

Since the scale factor λ is arbitrary, we choose $\lambda = g_{\text{min}}/2 = \mathcal{A}$, thereby setting

$$\left. \frac{df}{d\tilde{\tau}} \right|_{\tilde{\tau}=\frac{1}{2}} = \left. \frac{dB}{ds} \right|_{s=s_{\text{ac}}} - \left. \frac{dA}{ds} \right|_{s=s_{\text{ac}}}, \quad (41)$$

removing the dependence of $f(\tilde{\tau})$ on g_{min} . We now examine the time dependent Schrödinger equation for the single avoided crossing,

$$i \frac{\partial}{\partial \tilde{t}} |\psi\rangle = H_{\text{ac}}(\tilde{\tau}) |\psi\rangle. \quad (42)$$

To reparameterize in terms of $\tilde{\tau}$, we must multiply both sides by $\frac{\partial \tilde{t}}{\partial \tilde{\tau}}$ yielding

$$i \frac{\partial}{\partial \tilde{\tau}} |\psi\rangle = \frac{\partial \tilde{t}}{\partial \tilde{\tau}} H_{\text{ac}}(\tilde{\tau}) |\psi\rangle. \quad (43)$$

We now observe that, since $\tilde{\tau} = \frac{\tilde{t}}{\tilde{t}_f}$, $\frac{\partial \tilde{t}}{\partial \tilde{\tau}} = \tilde{t}_f$. We further observe that the only dependence of $H_{\text{ac}}(\tilde{\tau})$ on N comes through $\mathcal{A} = \frac{g_{\text{min}}}{2}$, therefore, if we set,

$$\tilde{t}_f = \frac{b}{g_{\text{min}}} \propto \sqrt{N}, \quad (44)$$

where b is a free parameter, we obtain a rescaled Schrödinger equation where we remove the global factor of g_{min} in H_{ac} by globally scaling the total time \tilde{t}_f by a factor proportional to g_{min}^{-1} , yielding

$$\begin{aligned} i \frac{\partial}{\partial \tilde{\tau}} |\psi\rangle &= \frac{b}{g_{\text{min}}} H_{\text{ac}}(\tilde{\tau}) |\psi\rangle \\ &= \frac{b}{2} [-\hat{\sigma}_x + f(\tilde{\tau})\hat{\sigma}_z] |\psi\rangle, \end{aligned} \quad (45)$$

which no longer depends on N .

The exact functional form of $f(\tilde{\tau})$ is determined by α in $A(\alpha, \beta, \tau)$ and $B(\alpha, \beta, \tau)$. We first determine the end points of the interpolation. For a quantum walk ($\alpha = 0$), it will be discontinuous such that the boundary conditions are obeyed but $f(\tilde{\tau}) = 0$ for $0 < \tilde{\tau} < 1$. For adiabatic quantum search ($\alpha = 1$), we follow the method used in [18] for the complete graph, applying it here to the avoided crossing model. We derive that

$$\frac{df(\tilde{\tau})}{d\tilde{t}} = \frac{1}{\epsilon \tilde{g}^2(\tilde{\tau})}, \quad (46)$$

which is analogous to Eq. (17) of Ref. [18]. From this, it follows that the optimal $f(\tilde{\tau})$ for an adiabatic passage through the avoided crossing is

$$f(\tilde{\tau}) = -\cot(\pi\tilde{\tau}), \quad (47)$$

The interpolation between QW and AQC must preserve the boundary conditions, $f(0) = -\infty$ and $f(1) = \infty$. It can be shown that

$$f(\tilde{\tau}, \alpha) = -\cot(\pi\tilde{S}(\tilde{\tau}, \alpha)), \quad (48)$$

where

$$\begin{aligned} \tilde{S}(\tilde{\tau}, \alpha) &= \frac{\tilde{\tau}(1-\tilde{\tau})}{2\tilde{\tau}(1-\alpha) + \alpha} + \tilde{\tau} \\ &\quad - \frac{\tilde{\tau}(1-\tilde{\tau})}{2(1-\tilde{\tau})(1-\alpha) + \alpha}, \end{aligned} \quad (49)$$

provides the correct form for mapping from our original interpolation $A(\alpha, \beta, \tau)$ and $B(\alpha, \beta, \tau)$ in Eq. (27). To complete the single avoided crossing model, we note that the total timescale in both the original problem and the rescaled version is determined by the minimum gap g_{\min}^{-1} , which is the same in both models therefore the mapping between the total time in the single avoided crossing model and the original hypercube search are the same, $\tilde{t}_f = t_f$.

In the scaling we derive above, all dependence of the runtime on the problem size N is contained within the scaling of \tilde{t}_f . This runtime rescaling is also independent of α . Rescaled time \tilde{t}_f remains proportional to \sqrt{N} , indicating that all the protocols achieve the optimal quadratic quantum speed up. Provided that for all α values the protocols also obtain a finite probability of finding the marked state, then the difference between the algorithm runtimes with different values of α will not depend on N , and the scaling of all of these algorithms will be optimal, differing only by constant factors which do not depend on N . Figure 9 illustrates that all protocols do in fact reach a success probability approaching one for suitable choice of runtime \tilde{t}_f . Therefore, for searching which can be mapped onto a single avoided crossing model, and where the position of the crossing is known (at least to a good approximation), there is a whole family of protocols which exhibit the same optimal scaling as QW or AQC protocols and continuously interpolate between the two.

C. Optimizing hybrid schedules for a single run

Having shown that hybrid protocols between QW and AQC maintain the quadratic quantum speed up, the next question is how to optimize over this continuum of hybrid schedules. This is about optimizing the prefactors that connect the scaling $\propto \sqrt{N}$ to the absolute run time t_f . Examining this will give us insight into how the different mechanisms of QW and AQC combine, and when

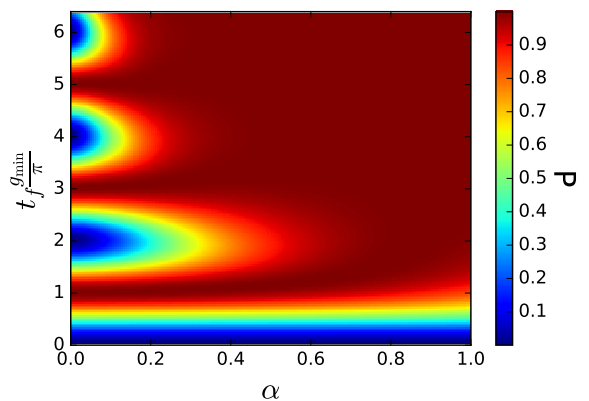


FIG. 9. Probability P of finding the marked state versus runtime t_f and interpolation parameter α for the single avoided crossing model.

it can be beneficial to use a combination of both. This optimization is by no means a secondary concern, since for practical implementations these prefactors can be the dominant factor [3].

A further crucial factor is how accurately the annealing schedule is specified in relation to the Hamiltonian parameters β and $s(\tau)$. In Sec. IID, we derived two schedules $s^{(o)}$ and $s^{(c)}$, both based on the two-level approximation, with the latter including a correction factor for the position of the minimum gap. We showed numerically in Sec. III C that $s^{(o)}$ performs poorly even for as few as $n = 8$ qubits, see Fig. 4. This suggests that, if the position of the minimum gap is not known accurately, it may be impossible to obtain a quantum speed up. We now examine the scaling of these two schedules to confirm this sensitivity to the position of the minimum gap. We also established in Sec. IV A that approximating the dynamics by considering only the two lowest energy eigenstates is a good approximation for more than about $n = 12$ qubits, and becomes increasingly accurate as n increases. We therefore use the rescaled single avoided crossing model from Sec. IV B for our analysis.

We first note that the gap calculated from the two-level approximation in Sec. IID is exactly the same as in the single avoided crossing model, since both are based only on the interactions of the two lowest energy levels, therefore, both will find the correct shape for the annealing protocol. We next observe that since the shift c calculated in the corrected version of the two-level approximation $s^{(c)}$ is the result of an exact calculation, so therefore the point β at which the schedule slows down will also be correct. Therefore, $s^{(c)}$ will obtain the \sqrt{N} scaling. Numerical results support this prediction in that for $n = 20$ the numerically calculated optimal schedule $s^{(n)}$ slows down at the same value as $s^{(c)}$ in Fig. 10. For $n = 5$ qubits the schedules are all distinct, while for $n = 20$, we see $s^{(c)} \simeq s^{(n)} \simeq 0.484$ where it is flattest, significantly different from $s^{(o)} = 0.5$.

To carry out the same calculation for $s^{(o)}$ where no cor-

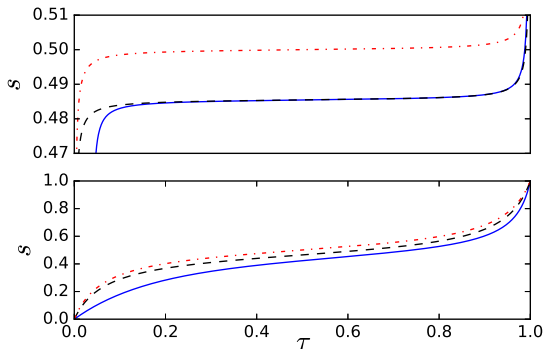


FIG. 10. (color online) Comparison of annealing schedules from Sec. II D for AQC searching over a hypercube of $n = 20$ qubits (top) and $n = 5$ qubits (bottom) for two-level approximation without shift $s^{(o)}$ (dotted), two-level approximation with shift $s^{(c)}$ (dashed), numerically calculated $s^{(n)}$ (solid). Note different scale for s in top figure.

rective shift is applied, we must modify the single avoided crossing model such that the minimum gap occurs at $f = \frac{0.5-\beta}{\mathcal{A}}$ rather than $f = 0$. To accomplish this, we substitute $f \rightarrow f'$ such that,

$$f'(\tau) = f(\tau) + \frac{0.5 - \beta}{\mathcal{A}} \quad (50)$$

substituting into Eq. (36) results in,

$$\hat{H}'_{ac}(\tilde{\tau}) = \mathcal{A} \left[\begin{pmatrix} 0 & -1 \\ -1 & 0 \end{pmatrix} + f(\tilde{\tau}) \begin{pmatrix} 1 & 0 \\ 0 & -1 \end{pmatrix} \right] + (0.5 - \beta) \begin{pmatrix} 1 & 0 \\ 0 & -1 \end{pmatrix}. \quad (51)$$

We now observe that for H'_{ac} , the rescaling in Eq. (45) does not leave the dynamics independent of N . For this rescaled version, the avoided crossing occurs at

$$\tilde{\tau}_\beta = \arctan \left(\frac{g_{\min}}{0.5 - \beta} \right) \quad (52)$$

It has been shown analytically in Ref. [21], and verified numerically in Fig. 7 and table I, that $0.5 - \beta$ will scale to zero as $1/n$, i.e., $1/\log(N)$. On the other hand, $g_{\min} \propto 1/\sqrt{N}$, therefore in the large N limit $\tilde{\tau}_\beta \propto \arctan \left\{ \frac{\log(N)}{\sqrt{N}} \right\}$. Hence

$$\left. \frac{\partial f}{\partial \tilde{\tau}} \right|_{\tilde{\tau}=\tilde{\tau}_\beta} \propto \frac{1}{\cos^2 \left(\arctan \left\{ \frac{\log(N)}{\sqrt{N}} \right\} \right)} \propto \frac{N}{\log^2(N)}. \quad (53)$$

² Note that the $O(n^{-2})$ factor in Eq. (12) of [21] becomes $O(n^{-1})$ using our conventions.

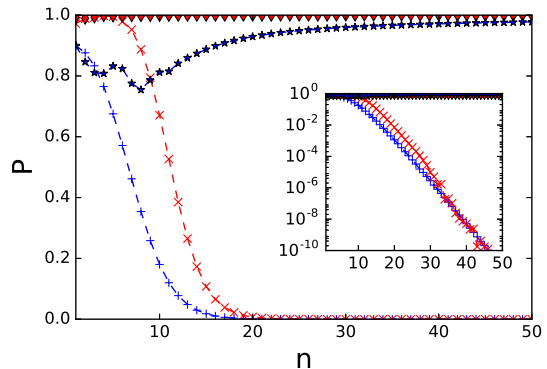


FIG. 11. (color online) Comparison of success probabilities P with annealing schedules $s^{(o)}$ and $s^{(c)}$ against number of qubits n . AQC (red) with runtime of $t_f = 4\pi/g_{\min}$ for $s^{(o)}$ (plus) and $s^{(c)}$ (diamond). QW (blue) with runtime of with $t_f = \pi/g_{\min}$ for $\gamma = 1$ and $s_\gamma = 1/2$ (plus) and for the shifted QW parameters (stars). Inset is the same, but with P on a logarithmic scale.

To keep the time spent around the avoided crossing, the scaled total runtime \tilde{t}_f needs to scale inversely with $\partial f/\partial \tilde{\tau}$ at τ_β as in Eq. (53). Therefore the total runtime will be $t_f \propto N/\log^2(N)$ $\tilde{t}_f \propto N\sqrt{N}/\log^2(N)$. This is worse than classical random guessing, indicating that the schedule $s^{(o)}$ based on the uncorrected two level approximation is unable to yield a quantum speed up for large N . Making use of the mapping of the hypercube Hamiltonian to the line from Sec. III B, this prediction is confirmed numerically in Fig. 11, which demonstrates that for a runtime proportional to \sqrt{N} , the success probabilities for both AQC and QW approach values close to one for sizes up to $n = 50$ for the schedule based on $s^{(c)}$, but success probabilities drop towards zero exponentially when using $s^{(o)}$.

This highlights an important difference between the hypercube and the fully connected graph. For the fully connected graph, successful AQC and QW strategies can be constructed by considering only the lowest two energy eigenstates. Although search on the hypercube is dominated by a single avoided crossing between the ground and first excited state, interactions with higher excited states must be taken into account to construct effective strategies. Based on the data in table I we can further deduce that this effect relates to the fact that the overlap of the manifold where the avoided crossing takes place with the marked state only approaches one polynomially in n (logarithmically in N). This slow approach allows the value of s at which the crossing occurs to be significantly different from the value predicted by the methods of [18]. This effective misspecification is sufficient to suppress a quantum speedup. Referring again to Fig. 10 shows the differences in the three schedules we consider as the number of qubits is scaled up. For 5 qubits all three schedules look different. By 20 qubits, the shifted schedule $s^{(c)}$ numerically calculated schedule $s^{(n)}$ are almost identical.

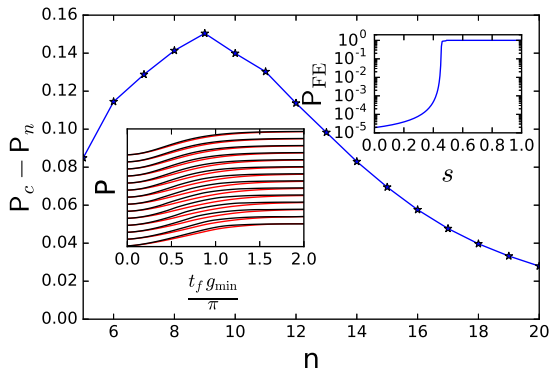


FIG. 12. (color online) Main figure: Difference in success probabilities $P_c - P_n$ between the annealing schedule calculated with the shifted two-level approximation $s^{(c)}$ and the numerically calculated schedule $s^{(n)}$ for a single run over a time π/g_{\min} . Lower Inset: Offset plot of the success probabilities P versus $t_f g_{\min}/\pi$ for $s^{(c)}$ (red) and $s^{(n)}$ (black). Upper Inset: Sum of the overlaps of $|E_1\rangle$ with $|m\rangle$ and $|\psi_{\text{init}}\rangle$ ($P_{\text{FE}} = |\langle E_1|m\rangle|^2 + |\langle E_1|\psi_{\text{init}}\rangle|^2$) against s for 20 qubits.

The difference between them around $\tau = 0.05$ is likely due to interactions with the higher excited states of the hypercube Hamiltonian early in the schedule. In the large system limit this difference will have little effect on the overall success probability, as the overlap with the initial ground state and the manifold of states participating in the avoided crossing approaches one exponentially fast in the number of qubits n (see table I).

However, the difference between $s^{(c)}$ and $s^{(n)}$ at early times in the run does affect their relative performance for small sizes, as Fig. 12 shows. Counterintuitively, $s^{(c)}$ does better than $s^{(n)}$ for around 10 qubits. The reason is that, while the gap is relatively small early in the schedule, so is the matrix element between the ground and first excited state of the marked state Hamiltonian. As a result, the numerically calculated schedule slows down unnecessarily in this region, as can be seen in Fig. 10 and the top inset of Fig. 12. The schedule $s^{(c)}$ assumes that the distance between the energy levels continues to grow linearly, and therefore does not slow down unnecessarily.

V. MULTIPLE RUNS FOR ONE SEARCH

A. Motivation

In a realistic setting of the search problem we can easily check whether the result of a search is the correct answer or not. Hence, we must consider not only single run strategies, but also multi-run strategies, where the success probability is defined as the probability of succeeding in at least one of several runs. In the context of quantum search on the hypercube, we measure which site of the hypercube our state is on, and then determine the energy of this state with respect to the search Hamiltonian. If

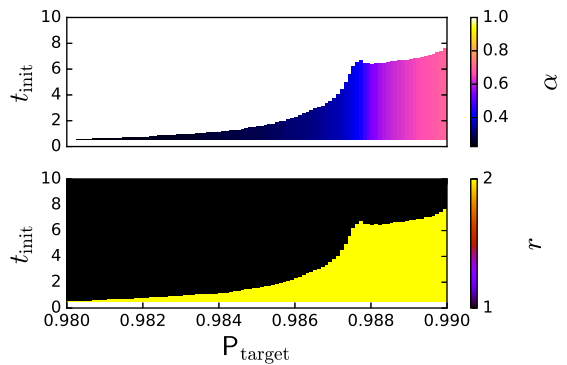


FIG. 13. (color online) Optimal number of runs (bottom) and optimal α (top) for the numerically optimized strategy $s^{(n)}$ with $n = 5$ qubits versus t_{init} and search success probability P . t_{init} is in inverse energy units, the same as t and τ on other figures.

this energy is zero, then we have found the state we are looking for, otherwise, we should re-initialize and run the search again. However, we also need to account for a non-zero ‘initialization’ time t_{init} associated with each run of the search. Such an initialization time is mathematically as well as physically necessary. The fidelity between the initial state and marked state $|\langle \psi_{\text{init}}|m\rangle|^2 = \frac{1}{N}$ is non-zero. An arbitrarily short run is equivalent to making a random guess. Therefore, without an additional penalty per run, it would be possible to guess an arbitrarily large number of times for free, thus finding the marked state in a total arbitrarily short time. Any physical device will take a significant amount of time both to setup the initial state and to measure the final state. For the purposes of our study, the effects on the total search time of initialization and readout times are the same, therefore the quantity we call t_{init} should be taken to include all of the time associated with a single run other than the actual runtime of the algorithm t_f , i.e., as including both initialization and measurement.

B. Multiple run searching

As an example, we consider five qubits using the numerically calculated optimal strategy $s^{(n)}$. Although the results are the same for the mapping to the line, due to the exact nature of the map, we perform this simulation on the full hypercube. For relatively high search success probabilities, between 0.98 and 0.99, the best single run strategy is to set $\alpha = 1$ and use the optimal AQC schedule. However, as Fig. 13 demonstrates, if t_{init} is short enough, the best strategy is two repeated runs of QW or intermediate protocols. Since the main point of multiple runs is to raise the search success probability close to one, this is the most relevant part of the parameter range, and it shows that hybrid strategies are useful here, when the position of the minimum gap is known accurately.

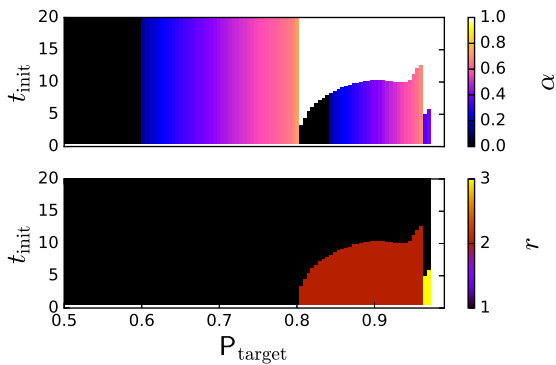


FIG. 14. Same as Fig. 13 but with the naive strategy $s^{(o)}$.

On the other hand, Fig. 14 shows that, if the same size search is considered but using the naive strategy $s^{(o)}$ without a corrective shift, then multi-run strategies are useful over a much wider range of search success probabilities, and even includes a region where the optimal strategy is to use three repeated runs. In this case, the ability to perform multiple repeated runs is used to partially correct for the fact that the annealing schedule is poorly constructed, although we emphasize that no multi-run strategy can enable this schedule to recover a quantum speed up for larger sizes. We return to the question of imperfect schedules in Sec. VI.

C. Noisy quantum searching

Another realistic situation where multiple runs can be helpful is when there is a significant level of unwanted decoherence or other forms of noise acting on the quantum hardware. In this case, shorter runs that end before decoherence effects are too strong, but consequently have lower success probabilities and hence need more repeats, may be able to maintain a quantum speed up. Decoherence effects on the different AQC and QW mechanisms are analysed in more detail in a related work [37].

We choose a simple yet instructive model of decoherence by adding a Lindblad term to the von-Neumann equation for the system density operator $\hat{\rho}(t)$,

$$\frac{\partial \hat{\rho}(t)}{\partial t} = -\frac{i}{\hbar} [\hat{H}(t), \hat{\rho}(t)] + \kappa \mathbb{P}[\hat{\rho}(t)], \quad (54)$$

where $\hat{H}(t)$ is the search Hamiltonian and $\kappa \mathbb{P}[\rho(t)]$ is a decoherence term tuned by a rate κ . We choose a form for \mathbb{P} that uniformly decays the coherences between states corresponding to vertices of the hypercube (the computational basis). This type of decoherence has been well-studied in the context of quantum walks [38–40] and, for high decoherence rate $\kappa \gg \gamma$, can be thought of as continuous measurement in the search space resulting in a quantum Zeno effect [41]. It is equivalent to coupling with an infinite temperature bath.

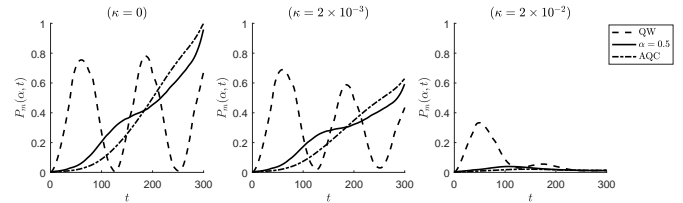


FIG. 15. Evolution of success probability $P(t) = \langle m | \rho(t) | m \rangle$ during a single search over the $n = 8$ hypercube, where m denotes the marked site. Figure 15 shows the evolution of $P(t)$ during a search over an 8-qubit hypercube graph. The broad effect of the decoherence is to reduce the instantaneous success probability towards a value of $1/N$, equivalent to classical guessing. The QW, AQC and hybrid search algorithms retain their characteristics up to an overall decoherence damping, which is independent of α . This suggests that the QW search, which spreads out more quickly over the search space, makes hybrid searches with more QW character better under decoherence. Indeed, for the higher decoherence rate in Fig. 15, only QW obtains a reasonable success probability. The AQC search relies on coherence sustained for longer times to reach high values of P .

We begin by looking at how the instantaneous success probability $P(t) = \langle m | \rho(t) | m \rangle$ evolves during a search, where m denotes the marked site. Figure 15 shows the evolution of $P(t)$ during a search over an 8-qubit hypercube graph. The broad effect of the decoherence is to reduce the instantaneous success probability towards a value of $1/N$, equivalent to classical guessing. The QW, AQC and hybrid search algorithms retain their characteristics up to an overall decoherence damping, which is independent of α . This suggests that the QW search, which spreads out more quickly over the search space, makes hybrid searches with more QW character better under decoherence. Indeed, for the higher decoherence rate in Fig. 15, only QW obtains a reasonable success probability. The AQC search relies on coherence sustained for longer times to reach high values of P .

To examine the performance of hybrid algorithms in more detail, first we consider single run searches with success probability $P(t_f, \alpha, \kappa)$. This is the final success probability of a hybrid search specified by α of duration t_f in the decoherence model of Eq. (54) with decoherence rate κ . We simulate the searches for durations $0 \leq t_f \leq 200$, and define the search duration that maximizes P for a particular choice of α and κ as $t_f^{(o)}$. We also define $\alpha^{(o)}$ as the value of α which maximizes $P(t_f^{(o)}, \kappa, \alpha)$, this corresponds to the search that reaches highest success probability for a given decoherence rate κ . Note that, for computational reasons, we limited α to the values 0.0, 0.1, 0.2... 0.9, 1.0 when performing the maximizations.

Figure 16 shows the results of this analysis for searches over a $n = 7$ dimensional hypercube graph. As the decoherence rate is increased, the hybrid searches which combine QW and AQC characteristics are able to reach slightly higher success probabilities P . The optimal hybrid schedule given by $\alpha^{(o)}$ reduces as the decoherence rate κ increases, confirming our hypothesis that QW is more useful for high decoherence rates, due to its faster spreading. At zero decoherence, a perfectly implemented AQC search can reach success probabilities arbitrarily close to one. Our simulations find that, for small values of κ we have $\alpha^{(o)} = 1$, i.e., AQC gives the highest success probability. As κ is increased, the highest-scoring search

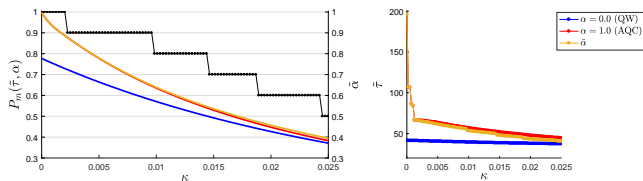


FIG. 16. (color online) Quantum searching on the $n = 7$ hypercube for QW (red), AQC (blue), and the hybrid search which yields the maximum P (orange) given by $\alpha^{(o)}$. Left: Probability of searches yielding the marked site $P(t_f, \alpha, \kappa)$ versus decoherence rate κ maximized over search times $0 \leq t_f \leq 200$. The value of $\alpha^{(o)}$ as κ varies is overlaid (black, right axis label). Note that α was limited to values in $0.0, 0.1, 0.2 \dots 0.9, 1.0$ for computational reasons. Right: The search time t_f which maximizes P versus κ .

changes and $\alpha^{(o)}$ decreases monotonically, indicating hybrid searches perform the best overall for intermediate levels of decoherence. In the limit of very high decoherence we are in a quantum Zeno effect regime which keeps the search in the initial superposition over all possible states. This means all searches will succeed with the same probability $P = |\langle \psi_{\text{init}} | m \rangle|^2 = 1/N$, equivalent to classical guessing. The usefulness of a search is also determined by how quickly it can be performed. The results for t_f in Fig. 16 (right) show that, while QW is never optimal for individual searches, it can be substantially quicker. This means that as the decoherence rate is increased, hybrid schedules take on more QW character and soon begin to achieve higher success probabilities than AQC in shorter search times.

Having characterized the effects of decoherence on a single run, we now consider multiple-run search strategies where each search is of the same duration t_f . We define the optimal annealing schedule as that which minimizes the time taken to reach a given success probability, optimized over all equal duration multiple-run search strategies, with durations of individual searches in the range $0 < t_f \leq 200$. There are three variables to optimize over: the success probability P , the initialization time between searches t_{init} , and the decoherence rate κ . We denote the number of runs by r , so the total search time is $t_f r$.

To make this multiple parameter optimization tractable, we considered a discrete set of values for $\alpha \in \{0.0, 0.1, \dots, 0.9, 1.0\}$. For a fixed value of $P = 0.95$, we then minimised the total search time $t_f r$ while varying t_{init} and κ . This is shown for a 7-dimensional hypercube in Fig. 17(a). There is a small threshold initialization time, below which the best strategy is to measure the system state as soon as it is prepared, at $t_{\text{init}} = 0$, indicating that our device can do no better than classical random guessing. There is little dependence on initialization time, other than this threshold. As κ is increased, there is a broad trend for more AQC-like searches to be optimal. However, this is punctuated with discontinuous changes to a QW search. The reason for this can be seen in Fig. 17(b), which shows, on the same axes, the number of

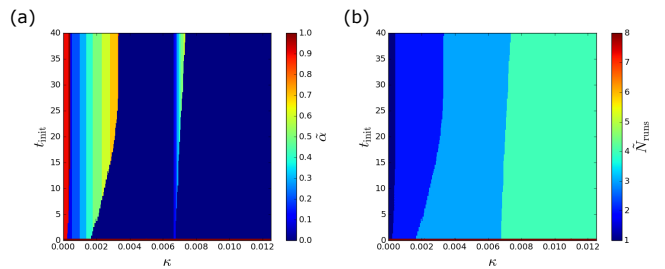


FIG. 17. (color online) (a) Anneal type parameter α which minimizes t_f as decoherence rate κ and initialization time t_{init} are varied. (b) Number of searches in the optimum multiple search strategy plotted on the same axes as (a). In the region of instantaneous measuring the number of runs is much greater than 6.

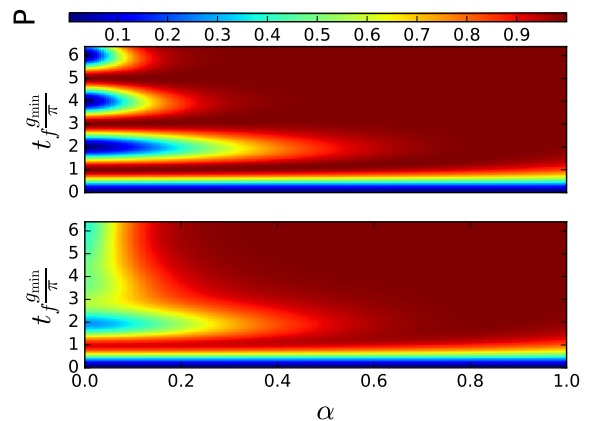


FIG. 18. Top: Probability P of finding the marked state versus runtime and α for the single avoided crossing model, same as Fig. 9 repeated for comparison. Bottom: Same as above with a 30% misspecification of the energy, $\Delta \mathcal{A}$.

runs r taken by the best performing multiple-run search algorithm. The boundaries where another run is required as κ is increased correspond exactly to the regions where the optimal value of α changes to 0. This transition arises when decoherence has increased such that the best performing search drops below $P = 0.95$, and so another run is required. However, the best hybrid search takes longer for larger α . Having an extra run means that a faster QW search with lower success probability for a single run is now sufficient to reach $P = 0.95$ for multiple runs. As the decoherence rate rises further, AQC is unable to outperform QW, as shown in Fig. 15, and the best strategy becomes as many QW runs as necessary to bring the total probability of success to $P = 0.95$.

VI. PROBLEM MISSPECIFICATION

A. Motivation

In addition to considering the effect of decoherence, it is also important to consider misspecification of the problem, for which the dynamics remain coherent, but some parameters are changed in unknown ways. Such a study is particularly relevant, given the critical difficulties which many classical analog computing efforts have faced due to propagation of errors [42]. Misspecifications can come about in a variety of ways, such as limited control precision, ignorance as to what the optimal parameters should be, or noise which is at a much lower frequency than the rate of the relevant quantum dynamics. An important example of the latter is so-called $\frac{1}{f}$ noise in superconducting qubit devices [43, 44], such as the quantum annealers constructed by D-Wave Systems Inc. It has been shown, for instance, that such misspecifications can cause AQC to give an incorrect solution on Ising spin systems [45], and effectively limit the maximum useful size of such devices. For our purposes, we will consider simple misspecification models in the large system limit, where the Hamiltonian can be mapped to a single avoided crossing in the form of Eq. (36). Because the initial and marked states are orthogonal in this limit, considering multiple runs which can be performed with negligible initialization time is not mathematically pathological. Furthermore, physically, we expect initialization and readout time to scale, at worst, polynomially with n , while runtime will scale as $\sqrt{N} \propto 2^{\frac{n}{2}}$. Therefore, in the large N limit, it is a very natural physical assumption that $t_f \gg t_{init}$. We first examine the effect of having the size of the minimum gap be misspecified, so that we do not know when to stop QW protocols, and then examine the effect of not knowing the position of the avoided crossing, which will cause QW protocols to use the wrong value of γ and AQC protocols to slow down at the wrong point in the annealing schedule. We have already seen in Sec. IV C that both of these can prevent the search algorithm from obtaining a quantum speed up.

To examine how these protocols perform numerically, we must consider not only the annealing schedule we use, but also the total time for which the protocol is run t_f . For simplicity, we will analyze this in the single avoided crossing model where we work in terms of the rescaled time $\tilde{\tau}$.

B. Error in gap size

We now examine the effect of misspecifying the size of the minimum gap. The effect of such misspecification can be approximated as an uncertainty in the total energy scale $\Delta\mathcal{A}$, which is mathematically equivalent to a misspecification of the total run time \tilde{t}_f . Assuming that the misspecification is distributed in a Gaussian manner

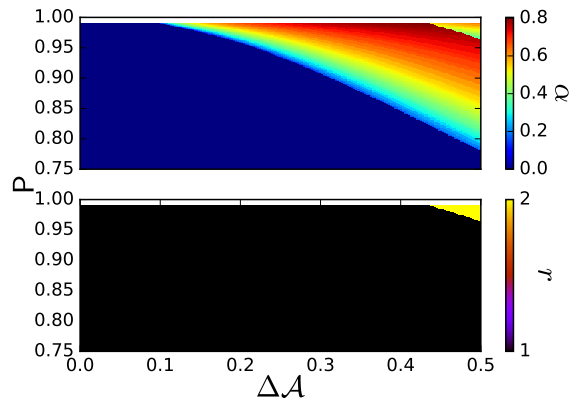


FIG. 19. (color online) Top: Optimal value of α versus success probability P and $\Delta\mathcal{A}$ from Eq. (55). Bottom: number of repeats r in optimal strategy versus P and $\Delta\mathcal{A}$.

around the intended runtime, the new success probability for a given anneal time t_f and α becomes

$$P(\tilde{t}_f, \alpha, \Delta\mathcal{A}) = \int_{-\infty}^{\infty} d\tilde{t}'_f \frac{P(|\tilde{t}'_f|, \alpha)}{\Delta\mathcal{A}\sqrt{2\pi}} \exp\left\{-\frac{(\tilde{t}'_f - \tilde{t}_f)^2}{2(\Delta\mathcal{A}\tilde{t}_f)^2}\right\}, \quad (55)$$

where $\Delta\mathcal{A}$ is the (unitless) fractional uncertainty in \mathcal{A} , and the absolute value in the argument of P within the integral is included to avoid negative time arguments.

Fig. 18 shows how the evolution makes a smooth transition between the characteristically sinusoidal behavior of success probability versus run time for QW, and the characteristically monotonic behavior of AQC. As the comparison between the perfect and misspecified cases demonstrates, gap misspecification causes a large reduction in the success probability of QW protocols, but has almost no effect on the monotonic AQC search. Fig. 19 illustrates that, for moderately high success probability and moderate amounts of misspecification of \mathcal{A} , the best protocol is no longer QW, but lies in between the optimal AQC schedule and QW. For large gap misspecification where a high success probability is required, the best approach is to run an intermediate strategy twice.

C. Error in avoided crossing location

Another type of problem misspecification is incorrectly specifying the position of the avoided crossing. To model this, we consider a modification of the problem Hamiltonian

$$\hat{H}'_{ac}(\tilde{\tau}, q) = \hat{H}_{ac} + q\mathcal{A}\hat{\sigma}_z. \quad (56)$$

This addition to the problem Hamiltonian is mathematically equivalent to performing a shift in the avoided crossing position $f(\tilde{\tau}) \rightarrow f(\tilde{\tau}) + q$ in Eq. (36). Based on this

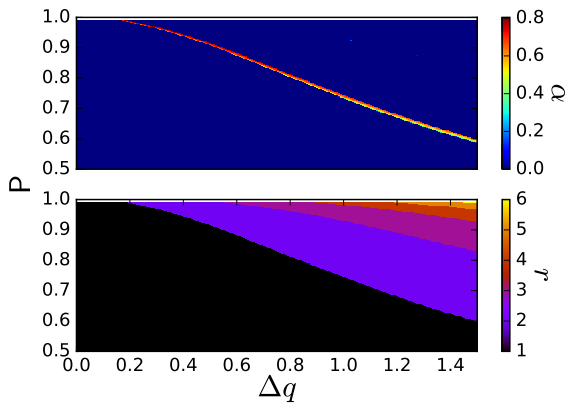


FIG. 20. (color online) Top: Optimal value of α versus success probability P and Δq from Eq. (57). Bottom: number of repeats r in optimal strategy versus P and Δq .

Hamiltonian, we define the success probability with misspecified avoided crossing position as

$$P(\tilde{t}_f, \alpha, \Delta q) = \int_{-\infty}^{\infty} dq \frac{P(\tilde{t}_f, \alpha, q)}{\Delta q \sqrt{2\pi}} \exp\left(-\frac{q^2}{2(\Delta q)^2}\right), \quad (57)$$

where Δq is the (unitless) fractional uncertainty in q , that controls the degree of misspecification. Figure 20 illustrates that, in contrast to gap misspecification, the best strategy is almost always QW. Intermediate strategies only become the superior method briefly, at the edge of the regime where single runs are the best way to reach the desired probability. At higher misspecification, multiple repeated QW become the best strategy.

The reason that gap size misspecification makes hybrid protocols ($\alpha > 0$) outperform QW for a large range of parameter space is because a QW can only succeed with a probability approaching one if $t_f \mathcal{A}$ is an odd multiple of π . The misspecification smears out these peaks and implies that the success probability of a QW will not approach one for any value of t_f . For protocols with some adiabatic character, however, the maximum success probability will still approach one as t_f becomes larger, as the adiabatic theorem holds for any finite gap. In fact, in half of the cases, the misspecified gap will actually be larger than in the case with no misspecification, and the performance of AQC will thus actually improve.

Misspecification in the avoided crossing position, on the other hand, does significant harm to both AQC and QW protocols. The success probability of a QW protocol performed with an incorrectly chosen γ does not approach one. Similarly, an AQC protocol with a poorly chosen schedule will require a much longer runtime for success probability to approach one.

VII. CONCLUSION

In this paper we have provided a detailed study of the scaling of quantum search on a hypercube graph using both quantum walk and adiabatic quantum search algorithms. Noting that these can be specified as two extremes of quantum annealing schedules, we have specified a family of quantum search algorithms that are hybrids between QW and AQC, and shown that the whole family achieves the \sqrt{N} quantum speed up. There are a number of subtleties in the scaling behavior on the hypercube that we treat in detail for short search times, complementing the work by Weibe and Babcock [30] on long timescales. In particular, we quantify the scaling with problem size of the minimum gap size, width, and position. While the position scales inversely with n , the size and width scale inversely with \sqrt{N} . This has implications for the precision with which the annealing schedule parameters must be specified in order to obtain a quantum speed up. While this is known in detail for quantum walk searching [21], our extension to the hypercube for AQC through hybrid QW-AQC schedules is an example of the advantages we gain by treating both QW and AQC as part of the same overall method of continuous-time quantum computing. Furthermore, under a range of realistic conditions we find that hybrid strategies intermediate between QW and AQC provide the best quantum search algorithm in this setting. This paves the way for hybrid algorithms to enhance the capabilities of near future quantum hardware. The techniques we use here can easily be extended to hybrid quantum search on other graphs, and to other quantum walk or adiabatic quantum computing algorithms.

Hybrid algorithms such as the ones we present here can be viewed as particular instances of quantum control techniques applied to solving optimization and search problems. Another application of quantum control to quantum algorithms is based on the Pontryagin minimum principle of optimal control: that optimal control protocols for solving these problems will follow a bang-bang scheme, with successive applications of the extreme values of the controls [46]. An algorithm based on such controls, called the Quantum Approximate Optimization Algorithm (QAOA), was first proposed by Farhi, Goldstone, and Gutmann [47, 48]. This protocol can be implemented either through digital quantum circuits, or by successively applied Hamiltonians. It has been shown that the QAOA can obtain an optimal \sqrt{N} scaling in solving the Grover search problem using a transverse field searching unitary [49], essentially the problem we consider in this paper.

There are two caveats which are worth noting in terms of the optimality of QAOA type bang-bang protocols. Firstly, when viewed as an application of successive Hamiltonians, these protocols require infinitely fast switching time, which is generally unphysical. Secondly, while the optimal control scheme to find the solution is mathematically always of a bang-bang form, this solu-

tion may exhibit Fullers phenomenon [50, 51], in which the optimal solution involves switching back and fourth between the two extremal Hamiltonians an infinite number of times in a finite time window. While mathematically valid, such a control scheme is clearly not physically realizable. It is an open question what happens to Hamiltonian based QAOA when finite switching time is added as a constraint. Our result that intermediate protocols between quantum walk and adiabatic protocols are still able to obtain an optimal speed up do provide an encouraging sign that QAOA may remain effective with realistic constraints applied.

In a recent study on solving permutation symmetric problems using ‘diabatic cascades’ [52, 53] finds that, deep in the diabatic regime, the dynamics are effectively classical. Muthukrishnan et al. focus only on changing the rate of evolution of an AQC algorithm. In contrast, we examine both the shape of the schedule and the rate of evolution. While it is likely that a similar diabatic cascade regime exists for very short total annealing times for all of the protocols we study as well, we leave this question to future studies.

As well as problem size, the performance of a quantum search in a realistic setting will depend on many other factors. By performing a fairly general and multi-faceted analysis of such factors, we uncover a landscape where no single protocol dominates. In asymptotically large systems with perfectly specified problems, a straightforward QW approach is best. However, this limit is ap-

proached slowly, since the success probability for QW scales only as n , i.e., logarithmically in problem size N . A rich structure exists for computationally interesting, non-asymptotic sizes. On the other hand, for asymptotically large systems with some degree of problem misspecification, interpolated protocols can outperform the QW approach. A simple open systems analysis reveals another layer of structure that can be exploited in realistic settings. For more discussion on the effects of noise and the competition between the mechanisms, see our related work [37]. In future work we will apply these techniques to algorithms with useful applications which can be run on near-future quantum hardware.

ACKNOWLEDGMENTS

We thank Patrick Scruby and Caleb Arthurs for checking the equations [any remaining errors are solely the authors’ responsibility]. NC and VK are supported by the UK Engineering and Physical Sciences Research Council Grant EP/L022303/1. SB has received funding for this research from the European Research Council under the European Unions Seventh Framework Programme (FP7/2007-2013)/ERC Grant agreement No. 308253 PACOMANEDIA. JGM acknowledges funding from the EPSRC Centre for Doctoral Training in Delivering Quantum Technologies at UCL.

-
- [1] J. Brooke, D. Bitko, T. F. Rosenbaum, and G. Aeppli, “Quantum annealing of a disordered magnet,” *Science* **284**, 779–781 (1999), <http://science.sciencemag.org/content/284/5415/779.full.pdf>.
- [2] M. W. Johnson, M. H. S. Amin, S. Gildert, T. Lanting, F. Hamze, N. Dickson, R. Harris, A. J. Berkley, J. Johansson, P. Bunyk, E. M. Chapple, C. Enderud, J. P. Hilton, K. Karimi, E. Ladizinsky, N. Ladizinsky, T. Oh, I. Perminov, C. Rich, M. C. Thom, E. Tolkacheva, C. J. S. Truncik, S. Uchaikin, J. Wang, and B. Wilson, “Quantum annealing with manufactured spins,” *Nature* **473**, 194–198 (2011).
- [3] Vasil S. Denchev, Sergio Boixo, Sergei V. Isakov, Nan Ding, Ryan Babbush, Vadim Smelyanskiy, John Martinis, and Hartmut Neven, “What is the computational value of finite-range tunneling?” *Phys. Rev. X* **6**, 031015 (2016).
- [4] T. Lanting, A. J. Przybysz, A. Yu. Smirnov, F. M. Spedalieri, M. H. Amin, A. J. Berkley, R. Harris, F. Altomare, S. Boixo, P. Bunyk, N. Dickson, C. Enderud, J. P. Hilton, E. Hoskinson, M. W. Johnson, E. Ladizinsky, N. Ladizinsky, R. Neufeld, T. Oh, I. Perminov, C. Rich, M. C. Thom, E. Tolkacheva, S. Uchaikin, A. B. Wilson, and G. Rose, “Entanglement in a quantum annealing processor,” *Phys. Rev. X* **4**, 021041 (2014).
- [5] Sergio Boixo, Vadim N. Smelyanskiy, Alireza Shabani, Sergei V. Isakov, Mark Dykman, Vasil S. Denchev, Mohammad H. Amin, Anatoly Yu Smirnov, Masoud Mohseni, and Hartmut Neven, “Computational multiqubit tunnelling in programmable quantum annealers,” *Nature Communications* **7** (2016), doi:10.1038/ncomms10327.
- [6] V.M. Kendon, N.C. Chancellor, S. Bose, and A. Daley, “Developing continuous-time quantum computing,” (2017), in preparation.
- [7] Michael Marzec, “Portfolio optimization: Applications in quantum computing,” in *Handbook of High-Frequency Trading and Modeling in Finance* (John Wiley & Sons, Inc., 2016) pp. 73–106.
- [8] G. E. Coxson C. R. Hill J. C. Russo, “Adiabatic quantum computing for finding low-peak-sidelobe codes,” (2014), presented at the 2014 IEEE High Performance Extreme Computing conference.
- [9] M. H. Amin E. Andriyash J. Rolfe B. Kulchytskyy R. Melko, “Quantum boltzmann machine,” arXiv:quant-ph:1601.02036 (2016).
- [10] M. Benedetti, J. Realpe-Gómez, R. Biswas, and A. Perdomo-Ortiz, “Estimation of effective temperatures in quantum annealers for sampling applications: A case study with possible applications in deep learning,” *Phys. Rev. A* **94**, 022308 (2016).
- [11] M. Benedetti, J. Realpe-Gómez, R. Biswas, and A. Perdomo-Ortiz, “Quantum-assisted learning of graphical models with arbitrary pairwise connectivity,” arXiv:1609.02542 (2016).

- [12] N. Chancellor, S. Zohren, P. Warburton, S. Benjamin, and S. Roberts, “A direct mapping of max k-sat and high order parity checks to a chimera graph,” *Scientific Reports* **6** (2016), 10.1038/srep37107, arXiv:1604.00651.
- [13] N. Chancellor, S. Szoke, W. Vinci, G. Aeppli, and P. A. Warburton, “Maximum-entropy inference with a programmable annealer,” *Scientific Reports* **6** (2016), doi:10.1038/srep22318.
- [14] Alejandro Perdomo-Ortiz, Neil Dickson, Marshall Drew-Brook, Geordie Rose, and Alan Aspuru-Guzik, “Finding low-energy conformations of lattice protein models by quantum annealing,” *Scientific Reports* **2** (2012).
- [15] L. K. Grover, “Quantum mechanics helps in searching for a needle in a haystack,” *Phys. Rev. Lett.* **79**, 325 (1997), ArXiv:quant-ph/9706033.
- [16] Charles H. Bennett, Ethan Bernstein, Gilles Brassard, and Umesh Vazirani, “Strengths and weaknesses of quantum computing,” *SIAM J. Comput.* **26**, 151–152 (1997).
- [17] Neil Shenvi, Julia Kempe, and K Birgitta Whaley, “A quantum random walk search algorithm,” *Phys. Rev. A* **67**, 052307 (2003), ArXiv:quant-ph/0210064.
- [18] J er mie Roland and Nicolas J. Cerf, “Quantum search by local adiabatic evolution,” *Phys. Rev. A* **65**, 042308 (2002).
- [19] Neil B. Lovett, Matthew Everitt, Robert M. Heath, and Viv Kendon, “The quantum walk search algorithm: Factors affecting efficiency,” *Math. Struct. in Comp. Sci.* (2015), arXiv:1110.4366v1[quant-ph], to appear (yes, really still pending!).
- [20] Thomas G. Wong and David A. Meyer, “Irreconcilable difference between quantum walks and adiabatic quantum computing,” *Phys. Rev. A* **93**, 062313 (2016).
- [21] Andrew Childs and Jeffrey Goldstone, “Spatial search by quantum walk,” *Phys. Rev. A* **70**, 022314 (2004), quant-ph/0306054.
- [22] S. Chakraborty, L. Novo, A. Ambainis, and Y. Omar, “Spatial search by quantum walk is optimal for almost all graphs,” *Physical Review Letters* **116** (2016).
- [23] Christopher Moore and Alexander Russell, “Quantum walks on the hypercube,” in *Proc. 6th Intl. Workshop on Randomization and Approximation Techniques in Computer Science (RANDOM ’02)*, edited by J. D. P. Rolim and S. Vadhan (Springer, 2002) pp. 164–178, quant-ph/0104137.
- [24] Trevor Lanting, “The d-wave 2000q processor,” (2017), presented at AQC 2017.
- [25] E. Farhi, J. Goldstone, S. Gutmann, and M. Sipser, “Quantum computation by adiabatic evolution,” (2000), quant-ph/0001106.
- [26] Nicholas Chancellor, “Max-k-sat, multi-body frustration, & multi-body sampling on a two local ising system,” AQC 2016 https://www.youtube.com/watch?v=aC-6hg_h3EA (2016).
- [27] Nicholas Chancellor and Viv Kendon, “Perturbative Hamiltonians from transverse Ising,” (2017), in preparation.
- [28] M. Born and V. Fock, “Beweis des adiabatsatzes,” *Z. Phys.* **51(3-4)**, 165–180 (1928).
- [29] Tameem Albash and Daniel A. Lidar, “Adiabatic quantum computing,” arXiv:1611.04471 (2016).
- [30] Nathan Wiebe and Nathan S Babcock, “Improved error-scaling for adiabatic quantum evolutions,” *New Journal of Physics* **14** (2012), 10.1088/1367-2630/14/1/013024.
- [31] M aria Kieferov a and Nathan Wiebe, “On the power of coherently controlled quantum adiabatic evolutions,” *New Journal of Physics* **16**, 123034 (2014).
- [32] “Python 2.7,” (2016), accessed August 10th, 2016.
- [33] “Python 3.5,” (2016), accessed August 10th, 2016.
- [34] “Numpy 1.11.1,” (2016), accessed August 10th, 2016.
- [35] “Scipy 0.17.1,” (2016), accessed August 10th, 2016.
- [36] “Matplotlib 1.5.1,” (2016), accessed August 10th, 2016.
- [37] J. G. Morley, N C. Chancellor, V. M. Kendon, and S. Bose, “Quench vs adiabaticity: balancing competing mechanisms for quantum search on noisy machines,” (2017), in preparation.
- [38] Gorjan Alagic and Alexander Russell, “Decoherence in quantum walks on the hypercube,” *Phys. Rev. A* **72**, 062304 (2005).
- [39] Peter C. Richter, “Quantum speedup of classical mixing processes,” *Phys. Rev. A* **76**, 042306 (2007).
- [40] Viv Kendon and Olivier Maloyer, “Optimal computation with non-unitary quantum walks,” *Theoretical Computer Science* **394**, 187 – 196 (2008).
- [41] B. Misra and E. C. G. Sudarshan, “The Zeno’s paradox in quantum theory,” *Journal of Mathematical Physics* **18**, 756–763 (1977), arXiv:arXiv:1011.1669v3.
- [42] Bissell C C, “A great disappearing act: the electronic analogue computer,” IEEE Conference on the History of Electronics (Bletchley, UK,) (2004).
- [43] Roger H. Koch, John Clarke, W. M. Goubau, J. M. Martinis, C. M. Pegrum, and D. J. van Harlingen, “Flicker (1/f) noise in tunnel junction dc squids,” *Journal of Low Temperature Physics* **51**, 207–224 (1983).
- [44] Roger H. Koch, David P. DiVincenzo, and John Clarke, “Model for 1/f flux noise in squids and qubits,” *Phys. Rev. Lett.* **98**, 267003 (2007).
- [45] Kevin C. Young, Robin Blume-Kohout, and Daniel A. Lidar, “Adiabatic quantum optimization with the wrong hamiltonian,” *Phys. Rev. A* **88** (2013).
- [46] Zhi-Cheng Yang, Armin Rahmani, Alireza Shabani, Hartmut Neven, and Claudio Chamon, “Optimizing variational quantum algorithms using ponyagin’s minimum principle,” *Phys. Rev. X* **7**, 021027 (2017).
- [47] Edward Farhi, Jeffrey Goldstone, and Sam Gutmann, “A quantum approximate optimization algorithm,” arXiv:1411.4028 (2014).
- [48] Edward Farhi, Jeffrey Goldstone, and Sam Gutmann, “A quantum approximate optimization algorithm applied to a bounded occurrence constraint problem,” arXiv:1412.6062 (2014).
- [49] Zhang Jiang, Eleanor G. Rieffel, and Zhihui Wang, “Near-optimal quantum circuit for grover’s unstructured search using a transverse field,” *Phys. Rev. A* **95**, 062317 (2017).
- [50] V. F. Borisov, “Fuller’s phenomenon: Review,” *Journal of Mathematical Sciences*, **100** (2000).
- [51] A. T. fuller, “Relay control systems optimized for various performance criteria,” in *Proc. First World Congress IFAC* (1960) pp. 510–519.
- [52] Siddharth Muthukrishnan, Tameem Albash, and Daniel A Lidar, “When diabatic trumps adiabatic in quantum optimization,” arXiv preprint arXiv:1505.01249 (2015).
- [53] Siddharth Muthukrishnan, Tameem Albash, and Daniel A. Lidar, “Tunneling and speedup in quantum optimization for permutation-symmetric problems,” *Phys. Rev. X* **6**, 031010 (2016).